

Rock Magnetic Evidence of Tectonic Control on the Sedimentation and Diagenesis in the Andaman Sea over ~ 1 Million Years

F. Badesab^{1*}, M.B.L. Mascarenhas-Periera¹, V. Gaikwad¹, P.Dewangan¹, P.P. Panda¹, K. Deenadayalan², K. Salunke¹, B. Augastian^{1,3}, J. R. Patil¹, and B.V. Lakshmi²

¹ CSIR- National Institute of Oceanography, Dona Paula-403004, Goa, India

² Indian Institute of Geomagnetism, New Panvel, Navi Mumbai-410208, India

³ School of Earth Sciences, Central University of Karnataka, Gulbarga, India

Corresponding author: Firoz Badesab (firoz@nio.org)

Abstract

We evaluate the sedimentary (magnetic, mineralogical, geochemical, grain size) records of a long sediment core (NGHP-01-17A) to elucidate the tectonic control on the sedimentation and diagenesis in the Andaman Sea (AS) over the past ~ 1 Ma. Two distinct sedimentary magnetic zones (Z-I and Z-II) are identified based on the rock magnetic signatures. A significant shift in the depositional environment is observed around ~ 90 ka which is marked by a rapid change in magnetite susceptibility (χ_{lf}), Fe, Ti and organic carbon content in Z-I. A trend of upward increase in χ_{lf} from ~ 90 ka to 3 ka in core NGHP-01-17A suggest increase in detrital flux to the AS and represents the onset of a new sedimentary regime following most recent event of tectonic uplift in Indo-Burman Ranges (IBR) which occurred at ~ 150 ka. Methane influenced progressive diagenetic dissolution of detrital iron oxides and subsequent precipitation of iron sulfides in Z-II is clearly evident in the rock magnetic and mineralogical data. Multiple bands of diagenetically formed iron sulfide nodules at different periods in Z-II indicate episodic intensification of anaerobic oxidation of methane (AOM) due to enhanced methane-flux. We propose that fluid migration forced by tectonic processes facilitated episodic release of methane from deep reservoir that led to the formation of iron-sulfide nodules in the AS.

Key words: Magnetic Minerals; Magnetic properties; Grain Size, Inorganic Geochemistry, Methane Hydrates, Iron Sulfide Nodules

Key points:

- A major shift in the depositional environment near ~ 90 ka is marked by a rapid change in magnetite concentration (χ_{lf}), Fe, Ti and organic carbon content. A trend of upward increase in χ_{lf} from ~ 90 ka to 3 ka in core NGHP-01-17A indicate increase in detrital flux to the Andaman Sea (AS) and represents the onset of a new sedimentary regime following most recent event of tectonic uplift in Indo-Burman Ranges (IBR) which occurred at ~ 150 ka.
- We provide evidence of tectonically-driven episodic fluid migration in the Andaman Sea (AS).
- Rock magnetic properties effectively recorded the geological processes that controlled sedimentation over ~ 1 Ma in the Andaman Sea.

1. Introduction.

The Andaman Sea (AS) is unique in terms of the complex tectonics, geology, climate and oceanography. Over geological time scales, tectonic activities coupled with changes in the strength of summer monsoon rainfall significantly influenced the physical and chemical weathering intensities, erosional processes in the source areas, and sediment depositional pattern in nearshore and Andaman Continental Shelf (ACS) (Awasthi et al., 2014; Cochran, 2010; Colin et al., 1998, 1999, 2006; Clift et al., 2008; Kuehl et al., 2019; Rashid et al., 2007). Tectonic uplift in the source areas coupled with climatic conditions provides important constraints on the evolution of marine sedimentary systems (Armitage et al., 2011; Zhang et al., 2018). Influence of tectonic activities and climatic changes on the Bengal fan sedimentation was unravelled using Sr-Nd (IODP-353; Peketi et al., 2021) and ^{10}Be (IODP-354; Lenard et al., 2020) isotopic compositions of the sediment cores. Exhumation and erosion of the Indo-Burman Ranges (IBR) followed by multi-phase upliftments (at ~8 Ma, ~3.6 Ma, ~2.6 Ma, 1.8–1.7 Ma, 1.2–0.6 Ma and 0.15 Ma) and sediment provenance changes in the AS have been reported (Li, 1995; Li et al., 1996, 2014; Najman et al., 2012; 2016; 2019, 2020; Zhang et al., 2015).

Previous studies documented the paleoceanographic and provenance related changes in the AS using mineralogical, elemental, inorganic geochemistry, sedimentological, isotopic, environmental magnetic, and foraminiferal records. Ali et al. (2015) observed no significant change in the sediment provenance in the AS during the past 60 ka. A linkage between variability in the sediment provenance, rapid deviation in the monsoon pattern, and changing pattern of ocean surface currents over 70 ka was also established (Awasthi et al., 2014). Changes in the weathering and erosion pattern in source regions and fluctuations in sediment contribution of terrigenous flux to the AS from the mid-late Holocene were controlled by climatic shifts, source area changes and tectonic processes (Achyuthan et al., 2014; Colin et al., 2006; Damodararao et al., 2016; Kuehl et al., 2019; Miriyala et al., 2017). Multi-proxy records of paleoclimatic, monsoonal and productivity changes are well-reported from the AS (Cao et al., 2015; Gebregiorgis et al., 2016; Kumar et al., 2018). Provenance, weathering pattern, erosion and monsoonal history in the Indo-Burman Ranges (IBR) and Indo-Burman-Arakan (IBA) of Myanmar over the past 21 ka were recorded in a sediment core from the AS (Colin et al., 2006; Najman et al., 2008, 2012). IBR and proximal volcanic sources were the major contributor of sediments in the AS during this period (Najman et al., 2019, 2020; Sebastian et al., 2019). A recent magnetic study on a sediment core from the AS spanning 21 ka tracked the provenance, weathering and history in IBR (Sebastian et al., 2019). They further established a

magnetic grain size based proxy to detect the intensities of chemical weathering and Indian summer monsoon (ISM) during the late glacial, early Holocene and mid-Holocene period (Sebastian et al., 2019). A comprehensive understanding of the Himalayan tectonic evolution was developed from the sedimentary records based on the interpretation of the isotopic data of detrital minerals (Najman, 2006). More recently, McNeill et al. (2017) closely examined the stratigraphic and chronostratigraphic data from Bengal fan and Ninetyeast Ridge. They highlighted that an interplay between tectonic, climatic and sedimentological processes in the Himalayan–Tibetan Plateau controlled the evolution of Bengal–Nicobar submarine fan sedimentation. The tectonic-sedimentary history of Gonjo Basin, southeast Tibet in response to India-Asia collision was constrained using magnetostratigraphy (Xiao et al., 2021). Control of climatic and tectonic activities on the Bengal fan sedimentation was recently revealed using Sr-Nd isotopic compositions of the Hole U1445A (International Ocean Discovery Program-353) from the western Bay of Bengal (Peketi et al., 2021). Despite the global importance of AS in context with strong tectonic and climatic forcing, detailed sediment records documenting the linkage between tectonics, changing fluvial supply, diagenesis and its sedimentary signal in marine sediments still remains elusive.

Marine sedimentary deposits from AS represent an important archive of how tectonic, climate and post-depositional (diagenetic) conditions have changed over geologic time. The storage and supply of sediments from source to marine sink depends on how landscape respond to climate and tectonic perturbations (Fildani et al., 2016). An understanding of the time lag between tectonic upliftment, erosion, transport and final sedimentation is important to track the climatic and tectonic signals in the marine sediment records (Burbank et al., 1996; Clift and Giosan, 2014; Kumar and Srivastava, 2017; Kumar et al., 2020). Sediments deposited in the AS potentially record the signatures of provenance changes due to upliftment, re-organization of drainage network (Colin et al., 1999; Najman et al., 2019, 2020), climatic conditions (Sebastian et al., 2019), sediment dispersal and accumulation (Kuehl et al., 2019), diagenetic processes (Kurian et al., 2008), and the evolution of Andaman Basin (Roy and Sharma, 1993). Geological setting assures a high supply of magnetic minerals to the AS through Irrawaddy, Salween and Sittang (ISS) rivers (Colin et al 1998; Licht et al., 2013; Robinson et al., 2007; 2014) and these minerals archive the signatures of source-to-sink related processes. A sediment core NGHP-01-17A (spanning ~ 1 Ma; Gebregiorgis et al., 2018) retrieved from the AS during the first Indian National Gas Hydrate Drilling Expedition preserves an excellent record and is well-suited for studying tectonic-controlled sediment depositional and diagenetic processes. In this study, we examined the sedimentary (magnetic, mineralogical, geochemical, grain size) records of a long sediment core (NGHP-01-17A) to elucidate the tectonic control on the sedimentation and

diagenesis in the AS over the past ~ 1 Ma. The present study provides the longest and most detailed sediment magnetic record available so far from the AS.

2. Materials and Methods

2.1. Geological Setting

The AS is located in a back-arc basin formed by the oblique subduction of the Indian Plate beneath the Sunda Plate (Kamesh Raju et al., 2007; Pal et al., 2003; Rodolfo, 1969a). The Andaman Island Arc complex is located within the central portion of the 5000 km long Burma-Sunda-Java subduction complex (Pal et al., 2003). The ISS are the major rivers, which efficiently transport the eroded continental sediments into the AS (Kurian et al., 2008). Estimated annual suspended sediment load supplied by the ISS river system is more than ~ 350 million tons to the Andaman Sea (Ramaswamy et al., 2004). The terrigenous sediments derived from ISS Rivers are routed through Gulf of Martaban to the deeper region of Andaman basin (Ramaswamy et al., 2004). Source rocks in the catchments areas of Irrawaddy River are dominated by Cretaceous-Cenozoic flysch of the IBR, Eocene-Miocene-Quaternary sediments of the Myanmar Central Basin, Late Precambrian, and Cretaceous-Eocene metamorphic/basic/ultrabasic rocks of the eastern Himalayas (Figure 1c; Bender, 1983; Robinson et al., 2014). The Salween and eastern tributaries of the Irrawaddy River drains through the Precambrian, Oligocene- Tertiary sedimentary, and acidic and metamorphic rocks of the eastern Shan Plateau (Robinson et al., 2007). The catchment areas of IBA and IBR receive heavy rains during the southwest (SW) monsoon (Garzanti et al., 2013). The sediments derived from these ranges are transported through several small rivers systems and get deposited along the western continental shelf of Myanmar (Garzanti et al., 2013; Kuehl et al., 2019). These sediments are further transported into the AS by the east flowing surface currents during the summer monsoon (Awasthi et al., 2014). Dominance of basaltic, granitic and sedimentary (shale) rocks in the source regions suggest that the geological setting around the AS assures a high supply of magnetic minerals to the study area through ISS rivers. An environmental magnetic investigation on a short sediment core (GC-3A) proximal to Site 17 (present core location) (Sebastian et al., 2019) and distal site (MD77-169, Sewell Seamount, Colin et al., 1998) reported that the sediment magnetic mineralogy is dominated by magnetite, titanomagnetite and hematite (Figure 1a,c).

2.2. Core Location and Age-Depth Model

As part of the Indian National Gas Hydrate Program (NGHP), a 700 m long sediment core NGHP-01-17A from Site 17 was collected onboard D/V JOIDES Resolution from the AS. The sediment

core NGHP-01-17A (10°45.1912'N, 93°6.7365'E) was raised from a water depth of 1356 m (Figure 1a) (Collett et al., 2008). Age model of the sediment core (NGHP-01-17A) was established by Gebregiorgis et al., 2018 using a high resolution benthic foraminifer (*C. wuellerstorfi* and *C. mundulus*) $\delta^{18}\text{O}$ record with equivalent features in the LR04 global benthic $\delta^{18}\text{O}$ isotope stack (Lisiecki and Raymo, 2005) using Analyseries (Paillard et al., 1996). Furthermore, age model was constrained by Accelerator Mass Spectrometry (AMS) ^{14}C dates on planktonic foraminifera (Gebregiorgis et al., 2018). An age-depth model is presented as supplementary Figure S1. Numerous volcanic ash layers were found in the sediment core NGHP-01-17A. Sediment lithology at this site is dominated by pelagic/hemipelagic sedimentation (Cawthern et al., 2014; Collett et al., 2008). Upper 50 m of the sediment core which spans ~ 1 Ma was used in the present study.

2.3. Sub-Sampling and Measurements

The sediment core was sampled at 5 cm interval which produced 594 sub-samples. Iron sulfide nodules were hand-picked from different sediment core depth intervals during sub-sampling.

2.4. Rock Magnetic and Sediment Electrical Resistivity Measurements

Sediment samples for bulk magnetic measurements were dried at 40 °C, weighed and packed in 25-mm cylindrical sample bottles at the paleomagnetic laboratory of CSIR-National Institute of Oceanography (CSIR-NIO), Goa, India. Frequency-dependent magnetic susceptibility measurements were performed using the Bartington MS2B dual frequency ($\chi_{\text{lf}} = 0.47$ kHz and $\chi_{\text{hf}} = 4.7$ kHz) susceptibility meter. Anhyseretic remanent magnetisation (ARM) was imparted using 100 mT AF field superimposed with a fixed DC bias field of 50 mT. Isothermal remanent magnetisation (IRM) of 700 mT, 1000 mT, and 2000 mT in the forward direction and -20, -30, -100, and -300 mT in the backward direction was imparted using MMPM10 pulse magnetizer. All remanences were measured using AGICO automatic JR-6A spinner magnetometer. Mass-normalized IRM acquired with a peak field of 2T is considered to be the saturation isothermal remanent magnetization (SIRM). S-ratio is calculated as the ratio between the IRM at -300mT and SIRM ($\text{IRM}_{-300\text{mT}}/\text{IRM}_{2\text{T}}$; Stober and Thompson, 1979). Specialized magnetic measurements were carried out at Environmental Magnetism Laboratory of Indian Institute of Geomagnetism, Panvel, India. Temperature dependence of magnetic susceptibility (χ -T) was measured in a field of 300 A/m at 875 Hz by a CS-3 furnace unit attached to an AGICO (KLY-4S) Kappabridge. Electrical resistivity measurements were made on the split cores using Wenner array onboard D/V JOIDES Resolution.

2.5. Sedimentological analyses

2.5.1. Sediment Grain Size Measurements

Sediment grain size was measured using a Laser Diffraction Particle Size Analyzer (Beckman Coulter LS 13320) at National Centre for Polar and Ocean Research (NCPOR), Goa, India. Prior to analysis, sediment samples were first desalinated and were later decarbonated using dilute HCl (1N). Sediment suspensions were treated with 10% H₂O₂ to remove organic carbon, and 300 mg of dispersing agent (sodium hexametaphosphate) was added to the suspension, which was then ultrasonicated before analysis. Grain size values are presented as volume %.

2.5.2. Mineralogical Analyses

Mineralogical and microscopy analyses were conducted on selected bulk sediment and iron sulfide nodule samples respectively. Hand-picked nodules were large enough to allow multiple analyses. The magnetic mineral components were identified using a Rigaku X-Ray Diffractometer (Ultima IV). The samples were run from 15° to 65° of 2θ at 1°/min scan speed using Cu Kα radiation (λ = 1.5414 Å). The composition of bulk sediments and iron sulfide nodules was determined using an energy dispersive X-ray spectroscopy (EDS) probe attached to the microscope. Electron microscopic observations were made on the iron sulfide nodules using scanning electron microscope (JEOL JSM-5800 LV). Images were captured in secondary electron imaging mode at energy levels between 15 and 20 keV). Chemical composition of the nodules was determined using an Oxford Instruments Ltd. INCA-300 X-ray energy dispersive spectrometer (EDS) attached to the SEM.

2.6. Sediment Geochemistry

Most of the elements reported in the study area were determined using Inductively Coupled Plasma Optical Emission Spectrometer (Perkin Elmer, OPTIMA 7300 DV Simultaneous ICP-OES) at CSIR-NIO, Goa, India. A total of 85 samples were analyzed by ICP-OES for the determination of Fe, Al, Ti, and K. Around 50 mg of bulk sediment sample was digested in 10 ml of acid mixture (HF, HNO₃ and HClO₄) in a proportion of 7:3:1 in a PTFE beaker by heating on a hotplate. Additional 5 ml of acid mixture was added to ensure complete dissolution (Chester and Hughes, 1967). The semi-dry solution was re-dissolved in 4 ml of 1:1 suprapure HNO₃ and subsequently diluted to 100 ml using deionized water. These solutions were analyzed using an ICP-OES for the analysis of Fe, Ti, Al and K. The accuracy of the data found better than ± 5 % was assessed by the International reference material (MAG-1 Marine Sediment and SGR-1 Green River Shale) of United States Geological Survey.

Major element such as Si concentration was determined for 39 samples using PANalytical X-ray Fluorescence Spectroscopy (XRF) Model Axios at NIO Goa, India. For XRF analyses, a two cm thick subsection at every 5 cm sediment interval was sampled through the entire core length. Salt free fraction of the 2-cm-thick subsections of the sediment core were used. About 2 grams of powdered sample was treated with 1N Hydrochloric (HCl) acid to remove the carbonates associated with the sediments. The decarbonated sediments were dried and powdered. An aliquot (~1.5g) of the decarbonated sample was heated in a hot air oven at 110°C for at least 12 hours. This moisture free sample (~ 0.55g) was mixed with 5.5 g of fusion mixture (A-100 Di-Lithium Tetra Borate with 0.07% Lithium Bromide) at a ratio of 1:10, homogenized, converted to melt at 1100°C in a platinum crucible (MiniFuse2) and allowed to cool to become a glass bead. Prepared glass beads were analyzed by XRF to determine the concentration of SiO₂, which is then converted to Si by using conversion ratio. Accuracy of the data was assessed using the international standard reference material (JMS-1) and found to be better than ± 5%.

The total organic carbon was analysed on bulk powdered samples by a flash dynamic combustion method using the Thermo Scientific FLASH 2000 Series Nitrogen and Carbon (CN) analyser at CSIR-NIO, Goa, India. The total inorganic content was determined using UIC CM 5014 Coulometer. The CaCO₃ weight per cent was calculated by multiplying the values of inorganic carbon with the ratio of molecular weight of CaCO₃ to C (i.e. 8.33). CaCO₃ % = Total Inorganic Carbon × (Molecular weight of CaCO₃/Atomic weight of Carbon; Johnson et al., 2014). The total organic carbon content was calculated by subtracting the total inorganic carbon from the total carbon.

3. Results

3.1. Rock Magnetic Properties of Sediment Core NGHP-01-17A

Two distinct magnetic zones were defined based on the down-core variations in χ_{lf} and SIRM (Figures 1b and 2a-2b). The uppermost magnetic zone (Z-1: ~ 90 ka to 3.0 ka) showed a trend of gradual decrease in magnetic susceptibility (χ_{lf}), and SIRM values indicating the downcore decrease in magnetic mineral concentration in this zone (Figures 2a and 2b). In Z-I (~ 90 ka to 3.0 ka), we observed mixed trend in magnetite concentration (χ_{lf}) and magnetic grain size diagnostic proxy (ARM/SIRM) downcore indicating the presence of both fine and coarse-grained magnetic particles in varying concentration in these samples (Figures 2a and 2c). The Z-II (~1021.79 ka to 91.92 ka) is marked by a notable decrease in magnetic mineral concentration as seen through lower values of χ_{lf} and SIRM compared to Z-I (Figures 2a and 2b). A systematic trend of downcore rise in ARM/SIRM in Z-II suggests the dominance of fine-grained magnetite or authigenic greigite (Figure 2c; Lin et al.,

2020; Rodelli et al., 2019). A bivariate plot of χ_{ARM} and χ_{lf} showed the magnetic grain-size dependency (Figure S2: King et al., 1982). In general, magnetic mineralogy diagnostic parameter (S-ratio) is close to unity, but showed drops at four different sediment ages (137.02 – 55.7 ka, 745.3 – 710.1 ka, and 783.07 – 776.1 ka, and 1004.1 – 999.8 ka) suggesting four episodes (marked by S1, S2, S3, and S4) of reduced supply of magnetic particles during these periods (Figure 2d).

3.2. Temperature-Dependent Magnetic Susceptibility Analyses

Temperature dependence of magnetic susceptibility (χ -T) has been widely used to determine changes in magnetic mineralogy of marine sediments (Liu et al., 2005). Temperature-dependent magnetic susceptibility (χ -T) curves for selected samples representing different depth intervals are shown in Figures 3a-3h. A sharp decrease in χ between 569°C and 605°C in majority of the samples imply that the bulk magnetic mineralogy is governed by titanomagnetite (Figures 3a-3h; Dunlop et al., 1997). A minor increase in χ between 309 °C and 522 °C could be either due to the presence of titanomagnetite with a wide range of Ti-contents (Lattard et al., 2006), or conversion of pyrite into magnetite during heating process (Hirt and Gehring, 1991; Passier et al., 2001; Figures 3a-3h). In the samples from low S-ratio zones (S1, S2), a major drop in χ at 630°C could be due to the presence of maghemite (Figures 3a and 3f).

3.3. Geochemical, Particle Size and Sediment Electrical Resistivity Data of Core NGHP-01-17A.

Two distinct patterns in the variation of geochemical parameters showing a major shift at ~ 90 ka are observed. The TOC and Fe contents are relatively high upto ~ 90 ka and decreases further downcore and showed less fluctuations (Figures 2f and 2g). CaCO₃ content is low in Z-I and showed large fluctuations in Z-II (Figure 2h). An interesting feature of high mean grain size and distinct low TOC and Fe content is noticed at ~ 783.07 ka (Figures 2e-2g). In the low S-ratio intervals, we noticed that zone S1 is marked by low TOC and Fe content, while S2 showed low TOC and high Fe content (Figures 2d, 2f, and 2g). The S3 is marked by increase in mean grain size and low TOC and Fe content (Figures 2d, 2e, 2f, and 2g), while S4 showed minor increase in mean grain size and low TOC content (Figures 2d, 2e, and 2f). The sediment core electrical resistivity varies between 0.31 to 1.43 Ω .m (Figure 2h). Six peaks of increased sediment resistivity were identified (Figure 2i). The reconstructed $\delta^{18}O_{sw}$ pattern showed weak monsoon during glacial maxima and a strong during interglacials (Figure 2j; Gebregiorgis et al., 2018).

Selected elemental profiles characterizing the sediments of core NGHP-01-17A are shown in Figure 4. Profiles of elemental abundances showed significant variations in sediment inputs. The CaCO_3 values range from 9.24 to 40.92 wt% over the last ~ 1Myr (Figure 4b). Two distinct trend in calcium carbonate content are identified. Within Z-I, majority of samples exhibit low and uniform values of CaCO_3 , while Z-II samples which showed relatively higher values and large fluctuations throughout (Figure 4b). Elemental profile showed a distinct variation between the Z-I and Z-II (Figures 4c-4f). Two elemental records representing terrigenous input (iron, titanium) showed major variations in Z-I and Z-II (Figures 4c-4d). Fe and Ti content are higher in Z-I compared to Z-II (Figures 4c-4d). Overall, the K profile showed downcore increase, but does not exhibit any clear trend (Figure 7e). Downcore decrease in Si content is seen with a major drop at ~ 291.54 ka (Figure 4f). A marked shift of increase in Si content is seen at ~349.13 ka followed by a trend of relatively high values which fairly remains uniform further downcore (Figure 4f). Interelemental ratios showed variations in Z-I and Z-II (Figures 4g-4h). We record a high Fe/K ratio which mimics Ti/Al ratio in Z-I (Figures 4g-4h). A systematic trend of increase in Ti/Al and Fe/K values from ~ 61.96 to 3.0 ka and ~ 85.6 to 3.0 ka respectively are seen (Figures 4g-4h). A gradual downcore decrease in Fe/K profile within Z-II is noticed (Figure 4h).

3.4. Scanning Electron Microscopy (SEM-EDS) and X-ray Diffraction (XRD) Analyses

Magnetic mineralogy diagnostic rock magnetic parameter (S-ratio) indicated that the bulk magnetic mineralogy is dominated by titanomagnetite (Figure 2d). SEM-EDS analyses support our rock magnetic observations and further confirm that titanomagnetite is the dominant magnetic mineral in the studied sediments. Detrital titanomagnetite (Figures 5a-5b) and titanohematite (Figure 5c) grains of various sizes and shapes were identified in Z-I based on the grain morphology and composition. Titanomagnetite grains in Z-I appears fresh, well preserved, and less altered (Figure 5a,b). EDS data for these grains indicate the presence of titanium, iron, silicon, and oxygen with minor traces of potassium, calcium, aluminum, and vanadium (Figure 5a,b). Diagenetically formed pyrite occur as fine (Figures 5d,e) as well as framboidal crystals (Figure 5f) in the magnetically reduced zone (Z-II). EDS data indicate the presence of iron and sulfur along with minor amounts of aluminium, calcium, and silicon (Figures 5d, e, and f). A skeletal type, most probably titanohematite grain, with quadrangle plate-like structure is noticed in Z-II (Figure 5c). Titanomagnetite grain (Figure 5g) showing features of partial diagenetic dissolution was found in the bottom-most sediment interval of Z-II (~1021.79 ka to 91.92 ka).

The X-ray diffraction curves of representative bulk sediment samples from Z-I and Z-II are shown in Figure 6. Quartz (Qz) and calcite (Ct) are the dominant minerals identified in all samples (Figures 6a-6l). XRD peaks also confirmed the presence of magnetite (M) and hematite (H) in minor amounts in all the samples (S1, S2, S3, S4) exhibiting low S-ratio (Figures 6g-6l). In all the analyzed iron sulfide nodules, pyrite (Py) and quartz (Qz) are common, while aluminium (Al) is generally present in all nodules (Figures 7a-7f). Elemental sulfur (S) was also abundant in all the samples. SEM-EDS data of nodules confirms the presence of diagenetically formed iron sulfide mineral (Py) of various sizes and shapes in the analyzed samples below present-day sulfate-methane transition zone (SMTZ) (31.98 mbsf, 40.65 mbsf, and 43.61 mbsf) (Figures 8g-8l). EDS data indicate the presence of sulfur and iron along with minor amounts of aluminium, and silicon (Figures 8j-8l).

3.6. Correlation between Magnetic, Geochemical and Sedimentological Parameters

We examined the bivariate data plots to evaluate the plausible constraints on the sediment properties (Figure 9). A good covariation between χ_{lf} and SIRM is observed only in Z-I samples. The difference between slopes of Z-I and Z-II reflects the presence of ferri- and paramagnetic type mineral assemblages in these samples respectively (Figure 9a). Z-II samples showed much lower values of χ_{lf} and SIRM indicating the reduction in concentration of ferrimagnetic minerals and also hint on the presence of either para or anti-ferromagnetic minerals (Figure 9a).

Two different trends exhibited by two distinct population of magnetic particles were observed in bivariate data plot between χ_{lf} and ARM/SIRM within Z-I (Figure 9b). Uppermost sediment interval (~34.32 ka to 3.0 ka) within Z-I is dominated by high χ_{lf} and shows trend of down-core fining in magnetic grain size (Figure 9b). Comparatively, lower sediment interval (~ 89.55 ka to 35.21 ka) exhibited relatively low χ_{lf} and showed a trend of down-core coarsening in magnetic grains (Figure 9b). In general, S-ratio ranges between 0.73 and 0.99 and show wide variations in χ_{lf} (Figure 2d and Figure 9c). Few samples from both zones exhibited low S-ratio indicating the presence of high coercive minerals (Figure 9c). Coupling between χ_{lf} and mean grain size is strong only for Z-I samples, with highest values of χ_{lf} dominated by coarse-grained magnetic particles (Figure 9d). Z-II samples showed much narrow range in χ_{lf} and wider variations in mean grain size (Figure 9d). Coupling between magnetic grain size and physical grain size is generally weak for all samples. (Figure 9e). As seen through magnetic parameters (Figures 2a, 2b), Z-II samples are dominantly composed of paramagnetic minerals. High Fe content in few Z-II samples (Figures 2g, 9f) might be due to the presence of paramagnetic minerals (chlorite, pyrite or clays). Based on these co-variations, two distinct groups exhibiting similar characteristic are identified (Figure 9f). Z-I samples are

relatively rich in Fe content and exhibited higher χ_{if} (Figure 9f), while few samples in Z-II showed relatively low χ_{if} and Fe content. A cross plots (Figures 9g-9h) between Fe/K (proxy for intensity of chemical weathering; Govin et al., 2012) and magnetic susceptibility (concentration dependent; Thompson and Oldfield, 1986) provided important constraints on the weathering and erosional process controlling the magnetic grain size variations within Z-I.

4. Discussion

4.1. Rock Magnetic and Geochemical Evidences of Tectonic Control on the Sedimentary Evolution of the Andaman Sea

Tectonic uplift in source regions coupled with regional monsoon climate may affect the sediment provenance by modifying the topography, erosion regime, reorganization of the river drainage pattern and sediment routing system and consequently provide major constraints on the evolution of sedimentary system (Armitage et al., 2011; Clift et al., 2002, 2010; 2017; Matenco and Haq, 2020; Najman et al., 2019, 2020; Tang et al., 2016; Zhang et al., 2018a). Previous studies have demonstrated that tectonic and climatic changes in the source regions can be very well inferred from sediment rock magnetic, geochemical, grain size, mineralogical, and chronological records. For instance, a dedicated mineral magnetic, geochemical, sedimentological and mineralogical studies recorded the signals of tectonic uplift in the Himalayan region (Phartiyal et al., 2003), southern Alborz Mountains, northern Iran (Ballato et al., 2008), Tibetan Plateau (Govin et al., 2018; Hu et al., 2019; Tan et al., 2020; Tang et al., 2016; Yang et al., 2019), Back-Arc Basins, Western Pacific Ocean (George DeVries Klein, 1985), Kumano basin, Japan (Shi et al., 2017), Izu–Bonin forearc, northwest Pacific (Robertson et al., 2018), Ganges-Brahmaputra-Meghna delta (Grimaud, J.-L., et al., 2017), Pannonian Basin, Hungary (E Thomó-Bozsó et al., 2002), and Al Rehaili area, Northern Jeddah, Saudi Arabia (Alqahtani and Khalil, 2019). More recently, Peketi et al (2021) revealed the control of climatic and tectonic activities on the Bengal fan sedimentation using Sr-Nd isotopic data of the hole U1445A from the western Bay of Bengal (Peketi et al., 2021).

Magnetic minerals are capable to record a wide variety of geological processes including tectonics, provenance, weathering/erosion and diagenetic changes (Hatfield and Maher, 2008, 2009; Oldfield et al., 1985). IBR situated in the southern branch of the Himalayan–Tibetan Plateau has undergone multiple upliftments including the rapid rise at ~8 Ma, ~3.6 Ma, ~2.6 Ma, 1.8–1.7 Ma, 1.2–0.6 Ma and 0.15 Ma (Li, 1995; Li et al., 1996, 2014; Najman et al., 2019, 2020). Geology of IBR is dominated by igneous, metamorphic, and sedimentary rocks (Robinson et al., 2007). A well-developed ISS river systems flowing through these terrains assure high supply of magnetic minerals

to the AS (Bender, 1983; Colin et al 1998; Kurian et al., 2008; Licht et al., 2013; Robinson et al., 2007; 2014). In the studied core, a significant shift in the depositional environment is observed around ~ 90 ka and is marked by rapid change in magnetite concentration (χ_{lf}), Fe, Ti and TOC content in Z-I (Figures 2a, 2f and Figures 4c-4d). A linkage between magnetic enhancement followed by compositional, chronological (detrital zircon U-Pb, Ar-Ar ages), and isotopic changes in the terrestrial and marine sediments with the shifting of source areas due to discrete erosional unroofing events and drainage reorganization constrained by tectonic uplift is well-established. For example, in the Bengal fan (Peketi et al., 2021), Indus Basin, Arabian Sea (Kumar et al., 2020), Kameng River Section, eastern Himalaya (Chirouze et al., 2013), Celano catchment, central Italy (Forzoni et al., 2014), Miocene foreland basin, northern Iran (Ballato et al., 2008), Nanga Parbat massif, western Himalaya (Clift, 2017), NW Borneo (Menier et al., 2019), and Gulf of Mexico (Smith et al., 2019). In context of regional geology of IBR, increased Fe and Ti content (Figures 4c-4d) observed in Z-I are mainly derived from the Late Precambrian and Cretaceous-Eocene metamorphic/basic/ultrabasic rocks (Bender 1983; Robinson et al., 2014). Age of most recent tectonic upliftment in the IBR is ~ 150 ka (Li and Fang, 1999; Li et al., 2014; Najman et al., 2006, 2008, 2012; Qingsong Z, 2000). A recent study based on high-resolution seismic, water column, sediment core, and chronology data delineated the control of tectonic and oceanographic processes on the sediment dispersal and accumulation off ISS delta (Kuehl et al., 2019), Bengal fan (Peketi et al., 2021), and Indus Basin, Arabian Sea (Kumar et al., 2020). A trend of upward increase in χ_{lf} from ~ 90 ka to 3 ka in core NGHP-01-17A indicate increase in detrital flux to the AS and represents the onset of a new sedimentary regime following most recent event of tectonic uplift in IBR which occurred at ~ 150 ka. A similar χ_{lf} enhancement accompanied by coarser grain size was recorded in the sediment core (IODP Site U1457) from Indus Fan, Arabian Sea (Kumar et al., 2020). They attributed the magnetic enhancement to the rapid change in erosional processes and sediment supply linked with tectonic-climatic interaction.

Drainage reorganization and sediment routing system provides important constraints on the evolution of source-to-sink depositional systems (Chirouze et al., 2013; Govin et al., 2018; Lenard et al., 2020; Najman et al., 2016). Hence the sedimentary record from those systems provide vital insights on the tectonic and climatic forcing on the sediment delivery to the marine basin (Kuehl et al., 2019; Lenard et al., 2020; Smith et al., 2019). Several studies reported that the rates of tectonic uplift coupled with monsoonal changes in the source region determines the time required to develop an efficient drainage system to produce large sediment load into the marine sinks. For example, delayed response of sedimentation and provenance changes in terrestrial and marine basin due to hinterland tectonics,

drainage evolution, and change in sediment routing system are well-recorded in the Bengal fan (Lenard et al., 2020; Peketi et al., 2021), Ganga-Brahmaputra drainage basin (Chirouze et al., 2013), Neogene Siwalik foreland basin of the Himalaya (Huyghe et al., 2014), off ISS delta (Kuehl et al., 2019), Central Myanmar Basin (Najman et al., 2019, 2020), Canada (Shugar et al., 2019), Gulf of Mexico (Smith et al., 2019), Back-Arc Basins of the Western Pacific (George DeVries Klein, 1985), and offshore western Norway (Sømme et al. 2019). Thermochronological and provenance based studies provided evidence on the multi-phase upliftment of IBR (Najman et al., 2006, 2019, 2020). Their findings revealed that tectonic upliftment in the IBR significantly modified the ISS drainage network and constrained the delivery of continental sediments to the AS (Cochran, 2010; Derry and Lanord, 1996; Kuel et al., 2019; Najman et al., 2019, 2020; Rodolfo, 1969b; Roy and Sharma, 1993; Zhang et al., 2015). Response of landscape to tectonic and climatic forcing control the source to sink sediment transfer (Fildani et al., 2016). Based on the detrital zircon U-Pb and (U-Th)/He dating analyses on the sediment cores from Mississippi deep-sea fan, Fildani et al. (2016) reported that the response of landscape to tectonic and climatic forcing controlled the sediment accumulation and movement. However the timing and magnitude of sediment storage can cause lag in the transfer of sediments from terrestrial to marine sink (Kumar et al., 2020; Romans et al. 2016). For instance, Clift and Giosan, 2014 reported largest time-lag in the Indus submarine fan sedimentation after the tectonic uplift in the Himalayan-Tibetan plateau (Clift et al., 2010; Jonell et al., 2017; Lavo and Avouac, 2001). We hypothesized that a time-lag between recent tectonic uplift in the source region (IBR ~ 150 ka; Li and Fang, 1999; Li et al., 2014; Qingsong Z, 2000;) and onset (~ 90 ka, present study) of increased sedimentation in Z-I (recorded through increase in χ_{lf} , Fe, Ti and TOC; Figures 2a, 2g, 2f, and 4d) could be attributed to the delay in sediment delivery caused by the development and re-organization of drainage basin, and sediment routing system of ISS rivers in IBR region after the recent uplift event (Najman et al., 2016; 2019, 2020). However additional chronological and numerical modelling (geomorphological, erosion and deposition of sediment) data over longer timescales is needed to clearly attribute the influence of tectonic forcing on the sedimentation in the AS. Increase in Fe and Ti content in Z-I (~ 90 ka – 3 ka) is also indicative of strong weathering and erosion induced by tectonic uplift in IBR and is well recorded in the elemental data (Figures 4c, 4d, 4g, and 4h). A bivariate plots (Figures 9b, 9g, 9h) between magnetic (ARM/SIRM; Sebastian et al., 2019) and inorganic geochemical (Fe, Fe/K, Ti/Al) based proxy parameters provided additional constraints on the weathering regime (Colin et al., 1998; Govin et al., 2012; Kissel et al., 2003) controlling the magnetic grain size variations within Z-I. Two distinct magnetic grain size populations (group-A and group-B) exhibiting different characteristic are identified (Figure 9a).

Samples from group-A are distinctly marked by higher χ_{lf} , Fe, Fe/K, Ti/Al and relatively lower ARM/SIRM values compared to group-B samples which showed relatively lower χ_{lf} , Fe, Fe/K, Ti/Al and higher ARM/SIRM values (Figure 9). Magnetic grain size proxy (ARM/SIRM; Evan and Heller, 2003) has been successfully utilized to identify the weathering regime (Kissel et al., 2003; Sebastian et al., 2019) and track the monsoonal changes (Colin et al., 1998). Relatively low χ_{lf} manifested by the dominance of coarser magnetic particles in group-B (~ 90 – 33.21 ka) samples within Z-I most likely reflect the period of increased physical weathering and erosion in the catchment (Figure 9b). Enhanced increase in the supply of fine-grained magnetic particles (as seen through elevated ARM/SIRM values; Figure 2c) manifested by high Ti/Al values (Figures 4g and 9h) in group-A (~ 34.32 – 3 ka) samples within Z-I is indicative of period of increased chemical weathering in IBR. This is also well reflected in bivariate plots between Fe/K versus χ_{lf} and Ti/Al versus χ_{lf} (Figures 9g-9h). Higher values of Fe/K (Figure 9g) in group A is also indicative of the presence of more humid climatic conditions within the catchment area (Mulitza et al., 2008).

Previous studies reported that decline in vegetation cover, aridification, intensification of erosion in the catchment areas during drier period could result in higher supply of detrital hematite (Clift et al., 2017; Hu et al., 2019; Phartiyal et al., 2003; Shen et al., 2017; Wan et al., 2010; Yang et al., 2016). Aridification has been attributed to the interaction between the uplift of the Tibetan Plateau and global cooling. For example, intense arid condition in central Asia induced by the uplift of the Tibetan Plateau has been established from multi-proxy records (Kutzbach et al., 1989; Li and Fang, 1999; Liu and Yin, 2002; Manabe and Terpstra, 1974; Tada et al., 2016). Four major episodes (S1, S2, S3, S4) of low S-ratio are identified in the studied core (Figure 2d). SEM-EDS observations on the magnetic particles S1 (~ 137.02 ka to 55.7 ka, Figure 5c) showed the presence of titanohematite grain which might have been formed either due to increased arid conditions in IBR (Clift, 2017; Hu et al., 2019; Phartiyal et al., 2003; Shen et al., 2017; Wan et al., 2010; Yang et al., 2016;) or progressive reductive dissolution of ferrimagnetic minerals at sulfidic fronts (Nowaczyk, 2011; Rodelli et al., 2018; 2019).

Presence of authigenically formed magnetic iron sulfides in S2 and S3 (magnetically reduced zone) is indicative of intense magnetic mineral diagenesis in Z-II (Figures 2a, 2b, Figures 5e-5f, Figures 8d-1). Multiple bands of diagenetically formed iron sulfide nodules at different periods in Z-II indicate episodic intensification of AOM due to enhanced methane-flux (Figure 8). Previous studies have reported that sedimentary greigite and pyrrhotite can also exhibit higher coercivities which could result in low S-ratio (Kars and Kodama, 2015; Horng, C.S., 2018). Authigenically formed

pyrite were noticed in S2 and S3 (Figures 5e-5f). We hypothesize that these low S-ratio intervals (S2, S3) contained previously formed authigenic ferrimagnetic iron sulfide (greigite), which were no longer stable and subsequently got converted into pyrite (Kars and Kodama, 2015a,b). Recent magnetic mineral diagenetic study by Gaikwad et al., 2021 reported similar mechanism explaining the transformation of greigite to pyrite in a newly discovered active methane seep site from the Bay of Bengal. The low S-ratio (S2, S3) intervals are also manifested by low χ_{lf} and SIRM values (Figure 2a and 2b) in Z-II and supports our interpretation.

4.2. Diagenetic Modulation of Magnetic Mineral Properties

Drilling and coring activities conducted under the aegis of first National Gas Hydrate Expedition -01 (NGHP-EXP-01), onboard D/V JOIDES Resolution confirmed the presence of subsurface gas hydrate deposits manifested in the form of a bottom simulating reflector (BSR) at Site 17 in the AS (Collett et al., 2008, Kumar et al., 2014). Gas hydrates occurred as pore-filling material ranging from disseminated to highly saturated in volcanic ash beds (Kumar et al., 2014; Winters et al., 2014). Sediment core NGHP-01-17A retrieved from potential gas hydrate bearing region (Site 17) provides a unique opportunity to reconstruct a long-term history of methane-influenced magnetic mineral diagenesis in the AS.

Diagenesis of magnetic mineral is one of the vital post-depositional factors which could significantly affect the sediment magnetic record. Detrital iron-bearing minerals reacts with hydrogen sulfide produced via bacterial mediated sulfate reduction processes or AOM and gets further transformed into iron sulfides (Berner, 1970; Canfield, 1989; Jørgensen, 1982). Changes in concentration, grain size and mineralogy of magnetic particles in core NGHP-01-17A from ~1021.79 ka to 504.4 ka appears to be largely influenced by methane-related diagenetic processes induced by AOM coupled sulfate reduction (Figures 2a-2d). Absence of diagenetically magnetic iron sulfides (pyrite, greigite, pyrrhotite) and nodules in Z-I suggests that diagenesis did not have any significant effect on the sediment magnetic record as confirmed through SEM-EDS and XRD data (Figures 5a-5b and Figures 6a, 6b, 6g, and 6h). Interestingly, Z-II is marked by distinct low χ_{lf} values and showed the presence of numerous bands of iron sulfide nodules below present-day SMTZ (> 504.46 ka) (Figure 8a and Figures 8d-8l). We propose that these nodules were probably formed as a result of multiple methane seepage events, which led to enhanced AOM-coupled sulfate reduction at different times (Figures 8d-8l; Dongen et al., 2007; Horng, 2018; Mei et al., 2018).

Past studies reported the presence of iron sulfides, greigite and pyrite in methane and gas hydrate bearing marine sediments. For example, in Nankai Trough (Kars and Kodama, 2015a,b), K-G basin

(Badesab et al., 2017, 2019; Dewangan et al., 2013), offshore Taiwan (Horng and Roberts, 2018), and Cascadia Margin (Housen and Musgrave, 1996; Larrasoana et al., 2007; Musgrave et al., 2006). Mineralogical (SEM-EDS and XRD) analyses of iron sulfide nodules from (Z-II) showed the presence of pyrite (Figures 7a-7f and Figures 8d-8l). However, we did not observe any signatures of greigite in our mineralogical data (Figures 7a-7f and Figures 8g-8l). Lack of greigite in these samples can be explained by the fact that previously formed greigite might have got converted into more stable paramagnetic pyrite due to increase sulfide concentration which favoured pyritization process to complete (Berner, 1984; Kars and Kodama, 2015b).

In gas hydrate settings, formation of SMTZ is primarily dependent on the sedimentation rate, intensity of upward-migrating methane fluxes from deeper sedimentary layers and downward diffusing sulfate concentration (Canfield and Berner, 1987). Occurrences of numerous bands of iron sulfide nodules in Z-II provide hints on the strong build-up of paleo-SMTZ fronts formed as a result of long durational AOM-coupled sulfate reduction controlled by enhanced methane flux at Site 17 (Figures 8d-8f, and Table-01). Similar iron sulfide nodules were reported in the sediment cores from Yungan Ridge, Taiwan (Horng, 2018) and Western Siberia (Rudmin et al., 2018). Previous studies have reported the concurrence of distinct magnetic susceptibility minima close to SMTZ for example, in Argentine continental slope and continental margin off Uruguay (Garming et al., 2005; Riedinger et al., 2005). They suggested that enhanced hydrogen sulfide produced at SMTZ led to the dissolution of magnetite and subsequent precipitation of paramagnetic pyrite and produced distinct minima in χ_{lf} . In marine sedimentary sequences from southwestern Taiwan, Kao et al. (2004) reported the occurrence of higher susceptibility peaks at SMTZ associated with presence of ferrimagnetic greigite formed as a result of limited availability of hydrogen sulfide, while enhanced concentration favoured the formation of pyrite. In core NGHP-01-17A, a distinct minima in χ_{lf} is near ~ 90 ka which is much shallower than the depth of present day-SMTZ (~ 504.46 ka). (Figure 2a). It is interesting to note that we did not observe any iron sulfide nodules or distinct change in χ_{lf} near present-day SMTZ (Figures 8a-8c). In fact the χ_{lf} were rather low and showed more uniformity in their variations (Figure 8a). Mineralogical diagnostic (XRD) data of the samples close to SMTZ revealed the presence of both magnetite and pyrite (Figure 6e).

Marine gas hydrate system is sensitive to changing pressure and temperature conditions, and tectonic forcing can cause the migration of gas hydrate stability zone (GHSZ) (Shi et al., 2017). Detailed mineral magnetic and electron microscopic study by Larrasoana et al. (2007) on a sediment core from Southern Hydrate Ridge, offshore Oregon suggested that migration of methane through the

sediment column could result in the formation of iron sulfide nodules. Their work highlighted that tectonically forced fluid migration can significantly affect the normal steady state diagenesis and favour the formation of nodules. The present-day SMTZ in core NGHP-01-17A is at ~ 25 mbsf (Figures 8b-8c). Eighteen bands containing diagenetically formed iron sulfide (pyrite) nodules were found to be spatially distributed below present-day SMTZ (Figures 8d-8l, and Table-01). A recent high resolution rock magnetic and electron microscopy study conducted by Shi et al., 2017 on IODP core Site C0002 in the Kumano Basin, Nankai Trough, Japan established the linkage between tectonically driven methane migration and formation of iron sulfides. They reported that tectonic activities in Kumano Basin triggered methane venting from deeper sediment layers and caused the formation of pyrite aggregates along sediment fractures/faults which acted as conduits for methane migration. Similar observations were reported from Southern Hydrate Ridge by Larrasoña et al. (2007). The sediment core NGHP-01-17A lies within a seismically active region and the sedimentary sequence at this site provides a record of volcanic activities in the AS (Kumar et al., 2014; Kamesh Raju et al., 2007). Recently, Rose et al. (2014) reported the occurrence of gas hydrates in numerous coarse-grained ash layers produced as a result of volcanic activity (Cawthern et al., 2010) in core NGHP-01-17A. High permeability offered by such coarse-grained ash layers provided conducive environment for the methane migration through sediment column and constitute a dominant host lithology for nucleation of gas hydrates at this site (Collett et al., 2008; Rose et al., 2014). Organic geochemistry and pressure-core studies confirmed the presence of abundant methane starting below SMTZ till the bottom of the cored sediment section in NGHP-01-17A (Collett et al., 2008). High electrical resistivity measured in the bottom part of the studied core (~ 954.74 - 924.46 ka) indicate increased gas hydrate saturations (Figure 2i) (Collet et al., 2008; Winters et al., 2014). Tectonically induced migration of methane and shifting of SMTZ front was recorded in pore-water geochemical profiles of sediment cores from the active Ganos Fault in the Sea of Marmara (Halbach et al., 2004) and U-Th dating of seep carbonates, Vestnesa Ridge, off West Svalbard, Arctic (Himmler et al., 2019). We hypothesize that tectonic activities at Site 17 might have facilitated the episodic release of methane from the deeper gas reservoir which caused multiple episodes of enhanced methane flux followed by AOM leading to precipitation of iron sulfide nodules at different intervals in Z-II (Figures 8d-8f, and Table-01). However, additional organic geochemistry investigations are warranted to further confirm this hypothesis.

A plausible mechanism is proposed to explain the controls on the evolution of sedimentary magnetic zones (Z-I, Z-II) over the past ~ 1 Ma based on the magnetic mineralogies, elemental composition, porewater geochemistry, grain size data, tectonic events and age –depth model (Figure 10). Z-I

represent the onset of a new sedimentary regime (~ 90 ka) following the most recent event of tectonic uplift in the IBR which occurred at ~ 150 ka. A trend of upward increase in χ_{lf} from ~ 90 ka to 3 ka in core NGHP-01-17A indicate increase in detrital flux to the AS. In Z-II, tectonically forced methane migration controlled the diagenesis of magnetic minerals which led to the significant dissolution of detrital iron oxides and subsequent transformation to iron sulfides (pyrite). This is clearly evident in the rock magnetic and SEM-EDS data (Figures 2, 5, and 6). Numerous bands of diagenetically formed iron sulfide nodules (Figure 7 and Figure 8) at different intervals in Z-II indicate episodic intensification of AOM due to enhanced methane-flux.

5. Conclusion

Rock magnetic, sedimentological, mineralogical and inorganic geochemistry data of sediment core (NGHP-01-17A) demonstrated the magnetic property variations are controlled by changes in the magnetite content, mineralogy, and grain size, which are linked to tectonic upliftment of the IBR (Z-I), aridification, and tectonically-induced fluid migration in the AS (Z-II). Major change in the depositional environment near ~ 90 ka is marked by rapid shift in magnetite concentration (χ_{lf}), Fe, Ti and organic carbon content in Z-I. Enhanced influx of detrital magnetic minerals from ~ 90 ka to 3 ka represents the onset of a new sedimentary regime following most recent event of tectonic uplift in the IBR which occurred at ~ 150 ka.

Multiple bands of diagenetically formed iron sulfide nodules at different periods in Z-II indicate episodic intensification of AOM due to enhanced methane-flux. We propose that fluid migration mainly driven by tectonic processes facilitated episodic release of methane from deep reservoir that led to the formation of iron-sulfide nodules in the AS. Rock magnetic properties effectively recorded the geological processes that controlled sedimentation over ~ 1 Ma in the Andaman Sea. A plausible conceptual model summarizing all possible constraints on the sedimentary evolution of the AS is developed in Figure10.

Acknowledgements

Authors are grateful to Director, CSIR-National Institute of Oceanography (NIO), for his support, and permission to publish this work. We thank ONGC, Panvel an esteem member of National Gas Hydrate Program coordinated by DGH for providing sediment core (NGHP-01-17A). The data used in this study can be made available upon email request to corresponding author. We thank Girish Prabhu and Areef Sardar for assistance with XRD and SEM-EDS analysis at CSIR-NIO. Aninda Mazumdar, B.N. Nath and Abhishek Saha are thanked for their timely inputs. We also thank the

Director, Indian Institute of Geomagnetism (IIG), New Panvel, for providing us permission to carry out specialized rock magnetic measurements. T.Ramprasad is thanked for helping us in obtaining necessary permission for accessing sediment core repository in Panvel. We thank Abhishek Tyagi from NCPOR, Vasco, Goa, India for providing assistance to carry out grain size analyses. The authors declare no conflict of interests. The work was performed under CSIR project MLP-1703 .

References

- Achyuthan, H., Nagasundaram, M., Gourlan, A. T., Eastoe, C., Ahmad, S. M., & Padmakumari, V. M. (2014). Mid-Holocene Indian Summer Monsoon variability off the Andaman Islands, Bay of Bengal. *Quaternary International*, 349, 232-244. doi.org/10.1016/j.quaint.2014.07.041
- Ali, S., Hathorne, E.C., Frank, M., Gebregiorgis, D., Stattegger, K., Stumpf, R., Kutterolf, S., Johnson, J.E. & Giosan, L. (2015). South Asian monsoon history over the past 60 ka recorded by radiogenic isotopes and clay mineral assemblages in the Andaman Sea. *Geochemistry, Geophysics, Geosystems*, 16(2), pp.505-521. doi.org/10.1002/2014GC005586
- Alqahtani, F., & Khalil, M. (2019). Geochemical analysis and tectonic evaluation of the Miocene–Pliocene sequence at Al Rehaili area, Northern Jeddah, Saudi Arabia. *Arabian Journal of Geosciences*, 12(10), 323. doi.org/10.1007/s12517-019-4491-0
- Armitage, J. J., Duller, R. A., Whittaker, A. C., & Allen, P. A. (2011). Transformation of tectonic and climatic signals from source to sedimentary archive. *Nature Geoscience*, 4(4), 231-235. doi.org/10.1038/ngeo1087
- Awasthi, N., Ray, J. S., Singh, A. K., Band, S. T., & Rai, V. K. (2014). Provenance of the Late Quaternary sediments in the Andaman Sea: Implications for monsoon variability and ocean circulation. *Geochemistry, Geophysics, Geosystems*, 15(10), 3890-3906. doi.org/10.1002/2014GC005462
- Badesab, F., Dewangan, P., Gaikwad, V., Kars, M., Kocherla, M., Krishna, K.S., Sangode, S.J., Deenadayalan, K., Kumar, P., Naikgaonkar, O., Ismaiel, M., & Khan, A. (2019). Magnetic mineralogical approach for exploration of gas hydrates in the Bay of Bengal. *Journal of Geophysical Research: Solid Earth* 24(5), 4428–4451. doi.org/10.1029/2019JB017466
- Badesab, F., Dewangan, P., Usapkar, A., Kocherla, M., Peketi, A., Mohite, K., Sangode, S.J., Deenadayalan, K. (2017a). Controls on evolution of gas-hydrate system in the Krishna-Godavari basin, offshore India. *Geochemistry, Geophysics, Geosystems*, 18(1), 52–74. doi.org/10.1002/2016GC006606
- Badesab, F., von Dobeneck, T., Briggs, R. M., Bryan, K. R., Just, J., & Müller, H. (2017b). Sediment dynamics of an artificially deepened mesotidal coastal lagoon: an environmental magnetic investigation of Tauranga Harbour, New Zealand. *Estuarine, Coastal and Shelf Science*, 194, 240-251. dx.doi.org/10.1016/j.ecss.2017.06.017

- Ballato, P., Nowaczyk, N. R., Landgraf, A., Strecker, M. R., Friedrich, A., & Tabatabaei, S. H. (2008). Tectonic control on sedimentary facies pattern and sediment accumulation rates in the Miocene foreland basin of the southern Alborz mountains, northern Iran. *Tectonics*, 27(6). doi.org/10.1029/2008TC002278
- Bender, F., (1983). *Geology of Burma*. Berlin-Stuttgart, Gebrüder Borntraeger, 293p.
- Berner, R. A. (1970). Sedimentary pyrite formation. *American Journal of Science*, 268(1), 1–23.
- Berner, R. A. (1984). Sedimentary pyrite formation: An update. *Geochimica et Cosmochimica Acta*, 48(4), 605–615. doi.org/10.1016/0016-7037(84)90089-9
- Burbank, D. W., Leland, J., Fielding, E., Anderson, R. S., Brozovic, N., Reid, M. R., & Duncan, C. (1996). Bedrock incision, rock uplift and threshold hillslopes in the northwestern Himalayas. *Nature*, 379(6565), 505-510. https://doi.org/10.1038/379505a0
- Canfield, D. E. (1989). Reactive iron in marine sediments. *Geochimica et Cosmochimica Acta*, 53(3), 619–632. doi.org/10.1016/0016-7037(89)90005-7
- Canfield, D. E., & Berner, R. A. (1987). Dissolution and pyritization of magnetite in anoxic marine sediments. *Geochimica et Cosmochimica Acta*, 51(3), 645–659. doi.org/10.1016/0016-7037(87)90076-7
- Cao, P., Shi, X., Li, W., Liu, S., Yao, Z., Hu, L., Khokiattiwong, S., & Kornkanitnan, N. (2015). Sedimentary responses to the Indian Summer Monsoon variations recorded in the southeastern Andaman Sea slope since 26 ka. *Journal of Asian Earth Sciences*, 114, pp.512-525. doi.org/10.1016/j.jseaes.2015.06.028
- Cawthorn, T., Johnson, J. E., Giosan, L., Flores, J. A., Rose, K., & Solomon, E. (2014). A late Miocene–early Pliocene biogenic silica crash in the Andaman Sea and Bay of Bengal. *Marine and Petroleum Geology*, 58, 490-501. doi.org/10.1016/j.marpetgeo.2014.07.026
- Cawthorn, T.R., Johnson, J., Bryce, J., Bilcert-toft, J., & Flores, J. (2010). A ~9.4 Ma ash record from the Andaman Accretionary Wedge: petrochemical implications for arc evolution. *American Geophysical Union Fall Meeting*. San Francisco, CA.
- Chirouze, F. O., Huyghe, P., Van Der Beek, P., Chauvel, C., Chakraborty, T., Dupont-Nivet, G., & Bernet, M. (2013). Tectonics, exhumation, and drainage evolution of the eastern Himalaya since 13 Ma from detrital geochemistry and thermochronology, Kameng River Section, Arunachal Pradesh. *Bulletin*, 125(3–4), 523–538. https://doi.org/10.1130/B30697.1
- Chu, N., Yang, Q., Liu, F., Luo, X., Cai, H., Yuan, L., Huang, J., and Li, J. (2020). Distribution of magnetic properties of surface sediment and its implications on sediment provenance and transport in Pearl River Estuary. *Marine Geology*, p.106162. doi.org/10.1016/j.margeo.2020.106162
- Clift, P. D., Hodges, K. V., Heslop, D., Hannigan, R., Van Long, H., & Calves, G. (2008). Correlation of Himalayan exhumation rates and Asian monsoon intensity. *Nature geoscience*, 1(12), 875-880. doi.org/10.1038/ngeo351

- Clift, P. D., Kroon, D., Gaedicke, C., & Craig, J. (2002). Tectonic and climatic evolution of the Arabian Sea region: an introduction. *Geological Society, London, Special Publications*, 195(1), 1-5. doi.org/10.1144/GSL.SP.2002.195.01.01
- Clift, P.D (2017). Cenozoic sedimentary records of climate-tectonic coupling in the Western Himalaya. *Progress in Earth and Planetary Science*. 4, 39. https://doi.org/10.1186/s40645-017-0151-8
- Clift, P. D., & Giosan, L. (2014). Sediment fluxes and buffering in the post-glacial Indus Basin. *Basin Research*, 26(3), 369-386. https://doi.org/10.1111/bre.12038
- Clift, P.D., Giosan, L., Carter, A., Garzanti, E., Galy, V., Tabrez, A.R., Pringle, M., Campbell, I.H., France-Lanord, C., Blusztajn, J. & Allen, C. (2010). Monsoon control over erosion patterns in the western Himalaya: possible feed-back into the tectonic evolution. *Geological Society, London, Special Publications*, 342(1), pp.185-218. https://doi.org/10.1144/SP342.12
- Cochran, J. R. (2010). Morphology and tectonics of the Andaman Forearc, northeastern Indian Ocean. *Geophysical Journal International*, 182(2), 631-651. doi.org/10.1111/j.1365-246X.2010.04663.x
- Colin, C., Kissel, C., Blamart, D., & Turpin, L. (1998). Magnetic properties of sediments in the Bay of Bengal and the Andaman Sea: impact of rapid North Atlantic Ocean climatic events on the strength of the Indian monsoon. *Earth and Planetary Science Letters*, 160(3-4), 623-635. doi.org/10.1016/S0012-821X(98)00116-2
- Colin, C., Turpin, L., Bertaux, J., Desprairies, A., & Kissel, C. (1999). Erosional history of the Himalayan and Burman ranges during the last two glacial–interglacial cycles. *Earth and Planetary Science Letters*, 171(4), 647–660. doi.org/10.1016/S0012-821X(99)00184-3
- Colin, C., Turpin, L., Blamart, D., Frank, N., Kissel, C., & Duchamp, S. (2006). Evolution of weathering patterns in the Indo-Burman Ranges over the last 280 ka: Effects of sediment provenance on $^{87}\text{Sr}/^{86}\text{Sr}$ ratios tracer. *Geochemistry, Geophysics, Geosystems*, 7(3). doi.org/10.1029/2005GC000962
- Collett, T., Riedel, M., Cochran, J. R., Boswell, R., Presley, J., Kumar, P., et al., & the NGHP Expedition 01 Scientists (2008). Indian National Gas Hydrate Program, Expedition - 01, Initial report, Directorate General of Hydrocarbons, Ministry of Petroleum and Natural gas, India.
- Damodararao, K., Singh, S. K., Rai, V. K., Ramaswamy, V., & Rao, P. S. (2016). Lithology, monsoon and sea-surface current control on provenance, dispersal and deposition of sediments over the Andaman continental shelf. *Frontiers in Marine Science*, 3, 118. doi.org/10.3389/fmars.2016.00118
- Derry, L. A., & France-Lanord, C. (1996). Neogene Himalayan weathering history and river $^{87}\text{Sr}/^{86}\text{Sr}$: impact on the marine Sr record. *Earth and Planetary Science Letters*, 142(1), 59-74.
- DeVries Klein, G. (1985). The control of depositional depth, tectonic uplift, and volcanism on sedimentation processes in the back-arc basins of the western Pacific Ocean. *The Journal of Geology*, 93(1), 1-25. doi.org/10.1086/628916

- Dewangan, P., Basavaiah, N., Badesab, F. K., Usapkar, A., Mazumdar, A., Joshi, R., & Ramprasad, T. (2013). Diagenesis of magnetic minerals in a gas hydrate/cold seep environment off the Krishna–Godavari basin, Bay of Bengal. *Marine Geology*, 340, 57–70. doi.org/10.1016/j.margeo.2013.04.016
- Dongen, B. E., Roberts, A. P., Schouten, S., Jiang, W. T., Florindo, F., & Pancost, R. D. (2007). Formation of iron sulfide nodules during anaerobic oxidation of methane. *Geochimica et Cosmochimica Acta*, 71(21), 5155–5167. doi.org/10.1016/j.gca.2007.08.019
- Dunlop, D. J., Özdemir, Ö., & Schmidt, P. W. (1997). Paleomagnetism and paleothermometry of the Sydney Basin 2. Origin of anomalously high unblocking temperatures. *Journal of Geophysical Research*, 102(B12), 27, 285–27,295. doi.org/10.1029/97JB02478
- Evans, M.E., & Heller, F. (2003). Environmental Magnetism: Principles and Applications of Enviromagnetics. *Academic Press, San Diego* (299 pp).
- Fildani, A., McKay, M. P., Stockli, D., Clark, J., Dykstra, M. L., Stockli, L., & Hessler, A. M. (2016). The ancestral Mississippi drainage archived in the late Wisconsin Mississippi deep-sea fan. *Geology*, 44(6), 479–482. . <https://doi.org/10.1130/G37657.1>
- Forzoni, A., Storms, J. E. A., Whittaker, A. C., & de Jager, G. (2014). Delayed delivery from the sediment factory: Modeling the impact of catchment response time to tectonics on sediment flux and fluvio-deltaic stratigraphy: Modeling delayed delivery from the sediment factory. *Earth Surface Processes and Landforms*. 39, 689–704. <https://doi.org/10.1002/esp.3538>
- Gaikwad V., Badesab, F., Dewangan, P., & Mahender, K. (2021). Diagenesis of Magnetic Minerals in Active/Relict Methane Seep: Constraints From Rock Magnetism and Mineralogical Records From Bay of Bengal. *Frontiers in Earth Science*, 9 (60), doi:10.3389/feart.2021.638594.
- Garming, J. F. L., Bleil, U., & Riedinger, N. (2005). Alteration of magnetic mineralogy at the sulfate–methane transition: Analysis of sediments from the Argentine continental slope. *Physics of the Earth and Planetary Interiors*, 151(3–4), 290–308. doi.org/10.1016/j.pepi.2005.04.001
- Garzanti, E., Limonta, M., Resentini, A., Bandopadhyay, P. C., Najman, Y., Andò, S., & Vezzoli, G. (2013). Sediment recycling at convergent plate margins (Indo-Burman ranges and Andaman–Nicobar Ridge). *Earth-Science Reviews*, 123, 113–132. doi.org/10.1016/j.earscirev.2013.04.008
- Gebregiorgis, D., Hathorne, E. C., Giosan, L., Clemens, S., Nürnberg, D., & Frank, M. (2018). Southern Hemisphere forcing of South Asian monsoon precipitation over the past~ 1 million years. *Nature communications*, 9(1), 1–8. doi.org/10.1038/s41467-018-07076-2
- Gebregiorgis, D., Hathorne, E. C., Sijinkumar, A. V., Nath, B. N., Nürnberg, D., & Frank, M. (2016). South Asian summer monsoon variability during the last~ 54 kas inferred from surface water salinity and river runoff proxies. *Quaternary Science Reviews*, 138, 6–15. doi.org/10.1016/j.quascirev.2016.02.012
- Govin, A., Holzwarth, U., Heslop, D., Ford Keeling, L., Zabel, M., Mulitza, S., Collins, J.A. & Chiessi, C.M., (2012). Distribution of major elements in Atlantic surface sediments (36 N–49 S): Imprint of terrigenous input and continental weathering. *Geochemistry, Geophysics, Geosystems*, 13(1). doi.org/10.1029/2011GC003785

- Govin, G., Najman, Y., Copley, A., Millar, I., Van der Beek, P., Huyghe, P., et al. (2018). Timing and mechanism of the rise of the Shillong Plateau in the Himalayan foreland. *Geology*, 46(3), 279–282. <https://doi.org/10.1130/G39864.1>
- Grimaud, J. L., Paola, C., & Ellis, C. (2017). Competition between uplift and transverse sedimentation in an experimental delta. *Journal of Geophysical Research: Earth Surface*, 122(7), 1339–1354. doi:10.1002/2017JF004239.
- Halbach, P., Holzbecher, E., Reichel, T., & Moche, R. (2004). Migration of the sulphate–methane reaction zone in marine sediments of the Sea of Marmara—can this mechanism be tectonically induced? *Chemical Geology*, 205(1-2), 73–82. doi.org/10.1016/j.chemgeo.2003.12.013
- Hatfield, R. G., & Maher, B. A. (2008). Suspended sediment characterization and tracing using a magnetic fingerprinting technique: Bassenthwaite Lake, Cumbria, UK. *Holocene*, 18, 105–115. doi.org/10.1177/0959683607085600
- Hatfield, R. G., & Maher, B. A. (2009). Holocene sediment dynamics in an upland temperate lake catchment: Climatic and land-use impacts in the English Lake District. *Holocene*, 19, 427–438. doi.org/10.1177/0959683608101392
- Hatfield, R. G., Cioppa, M. T., & Trenhaile, A. S. (2010). Sediment sorting and beach erosion along a coastal foreland: Magnetic measurements in Point Pelee National Park, Ontario, Canada. *Sedimentary Geology*, 231(3-4), 63–73. doi.org/10.1016/j.sedgeo.2010.09.007
- Himmler, T., Sahy, D., Martma, T., Bohrmann, G., Plaza-Faverola, A., Bünz, S., Condon, D.J., Knies, J., & Lepland, A. (2019). A 160,000-year-old history of tectonically controlled methane seepage in the Arctic. *Science advances*, 5(8), p.eaaw1450. DOI: 10.1126/sciadv.aaw1450
- Hirt, A. M., & Gehring, A. U. (1991). Thermal alteration of the magnetic mineralogy in ferruginous rocks. *Journal of Geophysical Research*, 96(B6), 9947–9953. doi.org/10.1029/91JB00573
- Horng, C. S. (2018). Unusual Magnetic Properties of Sedimentary Pyrrhotite in Methane-Seepage Sediments: Comparison with Metamorphic Pyrrhotite and Sedimentary Greigite. *Journal of Geophysical Research: Solid Earth*, 123, 4601–4617. doi.org/10.1002/2017JB015262
- Horng, C. S., & Roberts, A. P. (2018). The low-temperature Besnus magnetic transition: Signals due to monoclinic and hexagonal pyrrhotite. *Geochemistry, Geophysics, Geosystems*, 19, 3364–3375. doi.org/10.1029/2017GC007394
- Housen, B. A., & Musgrave, R. J. (1996). Rock-magnetic signature of gas hydrates in accretionary prism sediments. *Earth and Planetary Science Letters*, 139(3-4), 509–519. doi.org/10.1016/0012-821X(95)00245-8
- Hu, X., Chen, D., Pan, B., Chen, J., Zhang, J., Chang, J., Gong, C., & Zhao, Q. (2019). Sedimentary evolution of the foreland basin in the NE Tibetan Plateau and the growth of the Qilian Shan since 7 Ma. *Bulletin*, 131(9-10), pp.1744–1760. doi.org/10.1130/B35106
- Huyghe, P., van der Beek, P., Matthias, B., Catherine, C., Jean-Louis, M., Laurent, H., & François, C. (2014). Hinterland tectonics and drainage evolution recorded by foreland basin archives: the Neogene Siwaliks of the Himalaya, *Geophysical Research Abstracts*. V16, and EGU 2014-10409.

- Johnson, J.E., Phillips, S.C., Torres, M.E., Piñero, E., Rose, K.K., & Giosan, L. (2014). Influence of total organic carbon deposition on the inventory of gas hydrate in the Indian continental margins. *Marine and Petroleum Geology*, 58, 406–424. <https://doi.org/10.1016/j.marpetgeo.2014.08.021>.
- Jonell, T. N., Carter, A., Böning, P., Pahnke, K., & Clift, P. D. (2017). Climatic and glacial impact on erosion patterns and sediment provenance in the Himalayan rain shadow, Zaskar River, NW India. *Bulletin*, 129(7-8), 820-836. <https://doi.org/10.1130/B31573.1>
- Jørgensen, B. B. (1982). Mineralization of organic matter in the sea bed—The role of sulphate reduction. *Nature*, 296(5858), 643–645. doi.org/10.1038/296643a0
- Kamesh Raju, K. A., Murty, G. P. S., Amarnath, D., & Kumar, M. M. (2007). The west Andaman fault and its influence on the aftershock pattern of the recent megathrust earthquakes in the Andaman-Sumatra region. *Geophysical Research Letters*, 34(3). doi.org/10.1029/2006GL028730
- Kao, S. J., Horng, C. S., Roberts, A. P., & Liu, K. K. (2004). Carbon–sulfur–iron relationships in sedimentary rocks from southwestern Taiwan: Influence of geochemical environment on greigite and pyrrhotite formation. *Chemical Geology*, 203(1-2), 153–168. doi.org/10.1016/j.chemgeo.2003.09.007
- Karlin, R., & Levi, S. (1985). Geochemical and sedimentological control of the magnetic properties of hemipelagic sediments. *Journal of Geophysical Research: Solid Earth*, 90(B12), 10373-10392. doi.org/10.1029/JB090iB12p10373
- Kars, M., & Kodama, K. (2015a). Authigenesis of magnetic minerals in gas hydrate bearing sediments in the Nankai Trough, Offshore Japan. *Geochemistry, Geophysics, Geosystems*, 16, 947–961. doi.org/10.1002/2014GC005614
- Kars, M., & Kodama, K. (2015b). Rock magnetic characterization of ferrimagnetic iron sulfides in gas hydrate-bearing marine sediments at Site C0008, Nankai Trough, Pacific Ocean, off-coast Japan. *Earth, Planets and Space*, 67(1), 118. doi.org/10.1186/s40623-015-0287-y
- Kim, W., Doh, S. J., Yu, Y., & Lee, Y. I. (2013). Magnetic evaluation of sediment provenance in the northern East China Sea using fuzzy c-means cluster analysis. *Marine Geology*, 337, 9-19. doi.org/10.1016/j.margeo.2013.01.001
- King, J., Banerjee, S. K., Marvin, J., & Özdemir, Ö. (1982). A comparison of different magnetic methods for determining the relative grain size of magnetite in natural materials: some results from lake sediments. *Earth and Planetary Science Letters*, 59(2), 404-419. [https://doi.org/10.1016/0012-821X\(82\)90142-X](https://doi.org/10.1016/0012-821X(82)90142-X)
- Kissel, C., Laj, C., Clemens, S., & Solheid, P. (2003). Magnetic signature of environmental changes in the last 1.2 Myr at ODP Site 1146, South China Sea. *Marine Geology*, 201, 119–132. [https://doi.org/10.1016/S0025-3227\(03\)00212-3](https://doi.org/10.1016/S0025-3227(03)00212-3).
- Kuehl, S., Williams, J., Liu, P., Harris, C., Day, W.A., Tarpley, D., Goodwyn, M., & Yin, Y.A. (2019). Sediment dispersal and accumulation off the Ayeyarwady delta – tectonic and oceanographic controls. *Marine Geology*, 417. <https://doi.org/10.1016/j.margeo.2019.106000>.

- Kumar, P. K., Band, S. T., Ramesh, R., & Awasthi, N. (2018). Monsoon variability and upper ocean stratification during the last~ 66 ka over the Andaman Sea: Inferences from the $\delta^{18}\text{O}$ records of planktonic foraminifera. *Quaternary International*, 479, 12-18. doi.org/10.1016/j.quaint.2018.03.025
- Kumar, P., Collett, T.S., Boswell, R., Cochran, J.R., Lall, M., Mazumdar, A., Ramana, M.V., Ramprasad, T., Riedel, M., Sain, K. and Sathe, A.V. (2014). Geologic implications of gas hydrates in the offshore of India: Krishna–Godavari basin, Mahanadi basin, Andaman Sea, Kerala–Konkan basin. *Marine and petroleum geology*, 58, pp.29-98. oi.org/10.1016/j.marpetgeo.2014.07.031
- Kumar, A., & Srivastava, P. (2017). The role of climate and tectonics in aggradation and incision of the Indus River in the Ladakh Himalaya during the late Quaternary. *Quaternary Research*, 87(3), 363. https://doi.org/10.1017/qua.2017.19
- Kumar, A., Dutt, S., Saraswat, R., Gupta, A.K., Clift, P.D., Pandey, D.K., Yu, Z. & Kulhanek, D.K. (2020). A late Pleistocene sedimentation in the Indus Fan, Arabian Sea, IODP Site U1457. *Geological Magazine*, 157(6), pp.920-928. https://doi.org/10.1017/S0016756819000396
- Kurian, S., B. N. Nath, V. Ramaswamy, D. Naman, T. Gnaneshwar Rao, K. A. Kamesh Raju, K. Selvaraj, & Chen, C.T.A. (2008), Possible detrital, diagenetic and hydrothermal sources for Holocene sediments of the Andaman backarc basin, *Marine Geology*, 247(3), 178– 193. doi.org/10.1016/j.margeo.2007.09.006
- Kutzbach, J. E., Guetter, P. J., Ruddiman, W. F., & Prell, W. L. (1989). Sensitivity of climate to late Cenozoic uplift in southern Asia and the American west: numerical experiments. *Journal of Geophysical Research: Atmospheres*, 94(D15), 18393-18407. doi.org/10.1029/JD094iD15p18393
- Lavé, J., & Avouac, J. P. (2001). Fluvial incision and tectonic uplift across the Himalayas of central Nepal. *Journal of Geophysical Research: Solid Earth*, 106(B11), 26561-26591. https://doi.org/10.1029/2001JB000359
- Larrasoana, J. C., Roberts, A. P., Musgrave, R. J., Gràcia, E., Piñero, E., Vega, M., & Martínez-Ruiz, F. (2007). Diagenetic formation of greigite and pyrrhotite in gas hydrate marine sedimentary systems. *Earth and Planetary Science Letters*, 261(3-4), 350–366. doi.org/10.1016/j.epsl.2007.06.032
- Lenard, S. J. P., Lave, J., France-Lanord, C., Aumaitre, G., Bourles, D. L., & Keddadouche, K. (2020). Steady erosion rates in the Himalayas through late Cenozoic climatic changes. *Nature Geoscience*, 13, 448–452. https://doi.org/10.1038/s41561-020-0585-2
- Li, J., & Fang, X. (1999). Uplift of the Tibetan Plateau and environmental changes. *Chinese Science Bulletin*, 44(23), 2117-2124. doi.org/10.1007/BF03182692
- Li, J., (1995). Uplift of Qinghai-Xizang (Tibet) plateau and global change. *Univ. Press, Lanzhou*.
- Li, J., Fang, X., Song, C., Pan, B., Ma, Y., & Yan, M. (2014). Late Miocene–Quaternary rapid stepwise uplift of the NE Tibetan Plateau and its effects on climatic and environmental changes. *Quaternary Research*. 81(3), 400-423. doi.org/10.1016/j.yqres.2014.01.002
- Li, J., Xiaomin, F., Haizhou, M., Junjie, Z., Baotian, P., & Huailu, C. (1996). Geomorphological and environmental evolution in the upper reaches of the Yellow River during the late Cenozoic. *Science in China Series D-Earth Sciences*, 39(4), 380-390.

- Li, M., Zhu, S., Ouyang, T., Tang, J., & He, C. (2020). Magnetic fingerprints of surface sediment in the Bohai Sea, China. *Marine Geology*, 106226. doi.org/10.1016/j.margeo.2020.106226
- Licht, A., France-Lanord, C., Reisberg, L., Fontaine, C., Soe, A. N., & Jaeger, J. J. (2013). A palaeo Tibet–Myanmar connection? Reconstructing the Late Eocene drainage system of central Myanmar using a multi-proxy approach. *Journal of the Geological Society*, 170(6), 929-939. doi.org/10.1144/jgs2012-126
- Lisiecki, L. E., & Raymo, M. E. (2005). A Pliocene-Pleistocene stack of 57 globally distributed benthic $\delta^{18}\text{O}$ records. *Paleoceanography*, 20(1). doi.org/10.1029/2004PA001071
- Liu, Q., Deng, C., Yu, Y., Torrent, J., Jackson, M. J., Banerjee, S. K., & Zhu, R. (2005). Temperature dependence of magnetic susceptibility in an argon environment: implications for pedogenesis of Chinese loess/palaeosols. *Geophysical Journal International*, 161(1), 102-112. doi.org/10.1111/j.1365-246X.2005.02564.x
- Liu, Q., Roberts, A. P., Larrasoana, J. C., Banerjee, S. K., Guyodo, Y., Tauxe, L., & Oldfield, F. (2012). Environmental magnetism: principles and applications. *Reviews of Geophysics*, 50(4). doi.org/10.1029/2012RG000393
- Liu, X., & Yin, Z. Y. (2002). Sensitivity of East Asian monsoon climate to the uplift of the Tibetan Plateau. *Palaeogeography, Palaeoclimatology, Palaeoecology*, 183(3-4), 223-245. doi.org/10.1016/S0031-0182(01)00488-6
- Mack G.H. (1978) Tectonic control of sedimentation. In: Middleton G.V., Church M.J., Coniglio M., Hardie L.A., Longstaffe F.J. (eds) Encyclopedia of Sediments and Sedimentary Rocks. *Encyclopedia of Earth Sciences Series*. Springer, Dordrecht. doi.org/10.1007/978-1-4020-3609-5_235
- Maher, B. A., Watkins, S. J., Brunskill, G., Alexander, J., & Fielding, C. R. (2009). Sediment provenance in a tropical fluvial and marine context by magnetic ‘fingerprinting’ of transportable sand fractions. *Sedimentology*, 56(3), 841-861. doi.org/10.1111/j.1365-3091.2008.00999.x
- Manabe, S., & Terpstra, T. B. (1974). The effects of mountains on the general circulation of the atmosphere as identified by numerical experiments. *Journal of the atmospheric Sciences*, 31(1), 3-42. doi.org/10.1175/1520-0469(1974)031<0003:TEOMOT>2.0.CO;2
- Matenco, L. C., & Haq, B. U. (2020). Multi-scale depositional successions in tectonic settings. *Earth-Science Reviews*, 200, 102991. doi.org/10.1016/j.earscirev.2019.102991
- McNeill, L.C., Dugan, B., Backman, J., Pickering, K.T., Poudroux, H.F., Henstock, T.J., Petronotis, K.E., Carter, A., Chemale Jr, F., Milliken, K.L. & Kutterolf, S. (2017). Understanding Himalayan erosion and the significance of the Nicobar Fan. *Earth and Planetary Science Letters*, 475, pp.134-142. http://dx.doi.org/10.1016/j.epsl.2017.07.019
- Menier, D., Mathew, M., Pubellier, M., François S., Delcaillau, B., Siddiqui, N., Ram kumar, M., & M. Santosh. (2017). Landscape response to progressive tectonic and climatic forcing in NW Borneo: Implications for geological and geomorphic controls on flood hazard. *Scientific Report*. 7, 457. https://doi.org/10.1038/s41598-017-00620-y

- Mei, Z., Hongfeng, L., Hongxiang, G., Lihua, L., Daidai, W., & Nengyou, W. (2018). Methane seepage intensities traced by sulfur isotopes of pyrite and gypsum in sediment from the Shenhu area, South China Sea. *Acta Oceanologica Sinica*, 37(7), 20-27.
- Miriyala, P., Sukumaran, N.P., Nath, B.N., Ramamurty, P.B., Sijinkumar, A.V., Vijayagopal, B., Ramaswamy, V. and Sebastian, T. (2017). Increased chemical weathering during the deglacial to mid-Holocene summer monsoon intensification. *Scientific reports*, 7, p.44310. doi.org/10.1038/srep44310
- Mulitza, S., Prange, M., Stuut, J.B., Zabel, M., Von Dobeneck, T., Itambi, A.C., Nizou, J., Schulz, M. and Wefer, G., 2008. Sahel megadroughts triggered by glacial slowdowns of Atlantic meridional overturning. *Paleoceanography*, 23(4). doi.org/10.1029/2008PA001637
- Munack, H., Korup, O., Resentini, A., Limonta, M., Garzanti, E., Blöthe, J.H., Scherler, D., Wittmann, H. & Kubik, P.W. (2014). Postglacial denudation of western Tibetan Plateau margin outpaced by long-term exhumation. *Bulletin*, 126(11-12), pp.1580-1594. https://doi.org/10.1130/B30979.1
- Musgrave, R. J., Bangs, N. L., Larrasoaña, J. C., Gràcia, E., Hollamby, J. A., & Vega, M. E. (2006). Rise of the base of the gas hydrate zone since the last glacial recorded by rock magnetism. *Geology*, 34(2), 117–120. doi.org/10.1130/G22008.1
- Najman, Y. (2006). The detrital record of orogenesis: A review of approaches and techniques used in the Himalayan sedimentary basins. *Earth-Science Reviews*, 74(1-2), 1-72. https://doi.org/10.1016/j.earscirev.2005.04.004
- Najman, Y., Bracciali, L., Parrish, R. R., Chisty, E., & Copley, A. (2016). Evolving strain partitioning in the Eastern Himalaya: The growth of the Shillong Plateau. *Earth and Planetary Science Letters*, 433, 1–9. http://dx.doi.org/10.1016/j.epsl.2015.10.017
- Najman Y., Sobel E.R., Millar, I., Stockli, D.F., Govin, G., Lisker, F., Garzanti, E., Limonta, M., Vezzoli, G. Szymanski E., & Kahn A. (2019). The uplift of the Indo-Burman Ranges, Myanmar. *EGU General Assembly, Geophysical Research Abstracts*. Vol. 21, EGU2019-2959.
- Najman, Y., Sobel, E.R., Millar, I., Stockli, D.F., Govin, G., Lisker, F., Garzanti, E., Limonta, M., Vezzoli, G., Copley, A., & Zhang, P. (2020). The exhumation of the Indo-Burman Ranges, Myanmar. *Earth and Planetary Science Letters*, 530, p.115948. doi.org/10.1016/j.epsl.2019.115948
- Najman, Y., Bickle, M., BouDagher-Fadel, M., Carter, A., Garzanti, E., Paul, M., Wijbrans, J., Willett, E., Oliver, G., Parrish, R. & Akhter, S.H. (2008). The Paleogene record of Himalayan erosion: Bengal Basin, Bangladesh. *Earth and Planetary Science Letters*, 273(1-2), pp.1-14. https://doi.org/10.1016/j.epsl.2008.04.028
- Najman, Y., Allen, R., Willett, E.A.F., Carter, A., Barfod, D., Garzanti, E., Wijbrans, J., Bickle, M.J., Vezzoli, G., Ando, S. & Oliver, G. (2012). The record of Himalayan erosion preserved in the sedimentary rocks of the Hatia Trough of the Bengal Basin and the Chittagong Hill Tracts, Bangladesh. *Basin Research*, 24(5), pp.499-519. https://doi.org/10.1111/j.1365-2117.2011.00540.x

- Najman, Y., Bracciali, L., Parrish, R. R., Chisty, E., & Copley, A. (2016). Evolving strain partitioning in the Eastern Himalaya: The growth of the Shillong Plateau. *Earth and Planetary Science Letters*, 433, 1-9. <http://dx.doi.org/10.1016/j.epsl.2015.10.017>
- Nowaczyk, N. R. (2011). Dissolution of titanomagnetite and sulphidization in sediments from Lake Kineret, Israel. *Geophysical Journal International*, 187 (1), 34–44. doi:10.1111/j.1365-246X.2011.05120.x
- Oldfield, F., Maher, B. A., Donoghue, J., & Pierce, J. (1985). Particle-size related, mineral magnetic source sediment linkages in the Rhode River catchment, Maryland, USA. *Journal of the Geological Society*, 142, 1035–1046. doi.org/10.1144/gsjgs.142.6.1035.
- Paillard, D., Labeyrie, L., & Yiou, P. (1996). Macintosh program performs time-series analysis. *Eos, Transactions American Geophysical Union*, 77(39), 379-379. doi.org/10.1029/96EO00259
- Pal, T., Chakraborty, P. P., Gupta, T. D., & Singh, C. D. (2003). Geodynamic evolution of the outer-arc–forearc belt in the Andaman Islands, the central part of the Burma–Java subduction complex. *Geological Magazine*, 140(3), 289-307. doi.org/10.1017/S0016756803007805
- Passier, H. D., De Lange, G. J., & Dekkers, M. J. (2001). Magnetic properties and geochemistry of the active oxidation front and the youngest sapropel in the eastern Mediterranean Sea. *Geophysical Journal International*, 145(3), 604–614. doi.org/10.1046/j.0956-540x.2001.01394.x
- Peketi, A., Mazumdar, A., Pillutla, S. P. K., Sawant, B., & Gupta, H. (2021). Climatic and tectonic control on the Bengal fan sedimentation since the Pliocene. *Geochemistry, Geophysics, Geosystems*, 22, e2020GC009448. <https://doi.org/10.1029/2020GC009448>
- Perri, F., Critelli, S., Dominici, R., Muto, F., Tripodi, V., & Ceramicola, S. (2012). Provenance and accommodation pathways of late Quaternary sediments in the deep-water northern Ionian Basin, southern Italy. *Sedimentary Geology*, 280, 244-259. doi.org/10.1016/j.sedgeo.2012.01.007
- Phartiyal, B., Appel, E., Blaha, U., Hoffmann, V., & Kotlia, B. S. (2003). Palaeoclimatic significance of magnetic properties from Late Quaternary lacustrine sediments at Pithoragarh, Kumaun Lesser Himalaya, India. *Quaternary International*, 108(1), 51-62. doi.org/10.1016/S1040-6182(02)00193-3
- Poulton, S. W., Krom, M. D., & Raiswell, R. (2004). A revised scheme for the reactivity of iron (oxyhydr) oxide minerals towards dissolved sulfide. *Geochimica et cosmochimica acta*, 68(18), 3703-3715. doi:10.1016/j.gca.2004.03.012.
- Qingsong Z. (2000) Uplift and Environmental Changes of the Tibetan Plateau. In: Zheng D., Zhang Q., Wu S. (eds) Mountain Geoecology and Sustainable Development of the Tibetan Plateau. GeoJournal Library, vol 57. Springer, Dordrecht. <https://doi.org/10.1007/978-94-010-0965-2-2>
- Ramaswamy, V., Rao, P. S., Rao, K. H., Thwin, S., Rao, N. S., & Raiker, V. (2004). Tidal influence on suspended sediment distribution and dispersal in the northern Andaman Sea and Gulf of Martaban. *Marine Geology*, 208(1), 33-42. doi.org/10.1016/j.margeo.2004.04.019
- Rao, V. P., Kessarkar, P. M., Patil, S. K., & Ahmad, S. M. (2008). Rock magnetic and geochemical record in a sediment core from the eastern Arabian Sea: diagenetic and environmental implications during the late Quaternary. *Palaeogeography, Palaeoclimatology, Palaeoecology*, 270(1-2), 46-52. doi.org/10.1016/j.palaeo.2008.08.011

- Rao, V. P., Kessarkar, P. M., Thamban, M., & Patil, S. K. (2010). Paleoclimatic and diagenetic history of the late quaternary sediments in a core from the Southeastern Arabian Sea: Geochemical and magnetic signals. *Journal of oceanography*, 66(1), 133-146. doi.org/10.1007/s10872-010-0011-2
- Rashid, H., Flower, B. P., Poore, R. Z., & Quinn, T. M. (2007). A~ 25 ka Indian Ocean monsoon variability record from the Andaman Sea. *Quaternary Science Reviews*, 26(19-21), 2586-2597. doi.org/10.1016/j.quascirev.2007.07.002
- Riedinger, N., Pfeifer, K., Kasten, S., Garming, J. F. L., Vogt, C., & Hensen, C. (2005). Diagenetic alteration of magnetic signals by anaerobic oxidation of methane related to a change in sedimentation rate. *Geochimica et Cosmochimica Acta*, 69(16), 4117–4126. doi.org/10.1016/j.gca.2005.02.004
- Roberts, A. P. (2015). Magnetic mineral diagenesis. *Earth-Science Reviews*, 151, 1-47. doi.org/10.1016/j.earscirev.2015.09.010
- bertson, A.H., Kutterolf, S., Avery, A., Baxter, A.T., Petronotis, K., Acton, G.D., Carvallo, C. & Schindlbeck, J.C. (2018). Depositional setting, provenance, and tectonic-volcanic setting of Eocene–Recent deep-sea sediments of the oceanic Izu–Bonin forearc, northwest Pacific (IODP Expedition 352). *International Geology Review*, 60(15), pp.1816-1854. doi.org/10.1080/00206814.2017.1393634
- Robinson, R.A., Brezina, C.A., Parrish, R.R., Horstwood, M.S., Oo, N.W., Bird, M.I., Thein, M., Walters, A.S., Oliver, G.J., & Zaw, K. (2014). Large rivers and orogens: The evolution of the Yarlung Tsangpo–Irrawaddy system and the eastern Himalayan syntaxis. *Gondwana Research*, 26(1), pp.112-121. doi.org/10.1016/j.gr.2013.07.002
- Robinson, R.A.J., Bird, M.I., Oo, N.W., Hoey, T.B., Aye, M.M., Higgitt, D.L., Swe, A., Tun, T., & Win, S.L. (2007). The Irrawaddy river sediment flux to the Indian Ocean: the original nineteenth-century data revisited. *The Journal of Geology*, 115(6), pp.629-640.
- Rodolfo, K. S. (1969a). Bathymetry and marine geology of the Andaman Basin, and tectonic implications for Southeast Asia. *Geological Society of America Bulletin*, 80(7), 1203-1230. doi.org/10.1130/0016-7606 (1969)80[1203:BAMGOT]2.0.CO;2
- Rodolfo, K. S. (1969b). Sediments of the Andaman basin, northeastern Indian Ocean. *Marine Geology*, 7(5), 371-402.
- Romans, B. W., Castellort, S., Covault, J. A., Fildani, A., & Walsh, J. P. (2016). Environmental signal propagation in sedimentary systems across timescales. *Earth-Science Reviews*, 153, 7-29. https://doi.org/10.1016/j.earscirev.2015.07.012
- Rose, K., Johnson, J.E., Torres, M.E., Hong, W.L., Giosan, L., Solomon, E.A., Kastner, M., Cawthorn, T., Long, P.E., & Todd Schaefer, H. (2014). Anomalous porosity preservation and preferential accumulation of gas hydrate in the Andaman accretionary wedge, NGHP-01 site 17A. *Marine and Petroleum Geology*, 58(A), pp99-116. doi.org/10.1016/j.marpetgeo.2014.04.009.
- Roy, S. K., & Sharma, S. D. (1993). Evolution of Andaman Forearc Basin and its Hydrocarbon Potential. Proc. Second Seminar on petroliferous basins of India Vol. 1. 407-435

- Rudmin, M., Roberts, A.P., Horng, C.S., Mazurov, A., Savinova, O., Ruban, A., Kashapov, R., & Veklich, M. (2018). Ferrimagnetic iron sulfide formation and methane venting across the Paleocene-Eocene Thermal Maximum in shallow marine sediments, ancient West Siberian Sea. *Geochemistry, Geophysics, Geosystems*, 19(1), pp.21-42. doi.org/10.1002/2017GC007208
- Sandeep, K., Shankar, R., Warriar, A.K., Weijian, Z., & Xuefeng, L., (2015). The environmental magnetic record of palaeoenvironmental variations during the past 3100 years: a possible solar influence? *Journal of Applied Geophysics*. 118, 24–36. <https://doi.org/10.1016/j.jappgeo.2015.03.023>
- Sandeep, K., Shankar, R., Kumar, A., Yadava, M.G., Ramesh, R., Jani, R.A., Weijian, Z., & Xuefeng, L. (2017). A multi-proxy lake sediment record of Indian summer monsoon variability during the Holocene in southern India. *Palaeogeography, Palaeoclimatology, Palaeoecology*. 476, 1–14, <https://doi.org/10.1016/j.palaeo.2017.03.021>
- Sebastian, T., Nath, B.N., Venkateshwarlu, M., Miriyala, P., Prakash, A., Linsy, P., Kocherla, M., Kazip, A., & Sijinkumar, A.V. (2019). Impact of the Indian Summer Monsoon variability on the source area weathering in the Indo-Burman ranges during the last 21 ka—A sediment record from the Andaman Sea. *Palaeogeography, palaeoclimatology, palaeoecology*, 516, pp.22-34. doi.org/10.1016/j.palaeo.2018.11.035
- Shen, P., Zhang, L. M., Chen, H. X., & Gao, L. (2017). Role of vegetation restoration in mitigating hillslope erosion and debris flows. *Engineering Geology*, 216, 122-133. doi.org/10.1016/j.enggeo.2016.11.019
- Shi, M., Wu, H., Roberts, A.P., Zhang, S., Zhao, X., Li, H., Su, X., Yang, T., Chang, L., Hu, P., & Zhao, X. (2017). Tectonic, climatic, and diagenetic control of magnetic properties of sediments from Kumano Basin, Nankai margin, southwestern Japan. *Marine Geology*, 391, pp.1-12. doi.org/10.1016/j.margeo.2017.07.006
- Shugar, D., Clague, J., Best, J. L., Schoof, C., Willis, M.J., Copland, L., & Gerard H. R., (2017) River piracy and drainage basin reorganization led by climate-driven glacier retreat. *Nature Geoscience*. 10, 370–375. <https://doi.org/10.1038/ngeo293>
- Smith, T. M., Sundell, K. E., Johnston, S. N., Guilherme Andrade, C. N., Andrea, R. A., Dickinson, J. N., & Saylor, J. E. (2019). Drainage reorganization and Laramide tectonics in north-central New Mexico and downstream effects in the Gulf of Mexico. *Basin Research*. 32(3), 419–452. <https://doi.org/10.1111/bre.12373>
- Snowball, I. F. (1993). Geochemical control of magnetite dissolution in subarctic lake sediments and the implications for environmental magnetism. *Journal of Quaternary Science*, 8(4), 339-346. doi.org/10.1002/jqs.3390080405
- Sømme, T.O., Helland-Hansen, W., & Granjeon, D. (2009). Impact of eustatic amplitude variations on shelf morphology, sediment dispersal, and sequence stratigraphic interpretation: Icehouse versus greenhouse systems: *Geology*. 37, 587–590. <https://doi.org/10.1130/G25511A.1>.
- Stober J.C. and Thompson, R. (1979). An investigation into the source of magnetic minerals in some Finnish lake sediments, *Earth and Planetary Science Letters*. 45, 464–474. [https://doi.org/10.1016/0012-821X\(79\)90145-6](https://doi.org/10.1016/0012-821X(79)90145-6)

- Tada, R., Zheng, H., & Clift, P. D. (2016). Evolution and variability of the Asian monsoon and its potential linkage with uplift of the Himalaya and Tibetan Plateau. *Progress in Earth and Planetary Science*, 3(1), 4. doi.org/10.1186/s40645-016-0080-y
- Tan, M., Zhang, W., Fang, X., Yan, M., Zan, J., & Zhang, T. (2020). Rock magnetic record of core SG-3 since 1 Ma in the western Qaidam Basin and its paleoclimate implications for the NE Tibetan Plateau. *Palaeogeography, Palaeoclimatology, Palaeoecology*, 109949. doi.org/10.1016/j.palaeo.2020.109949
- Tang, Z., Yang, S., Qiao, Q., Yin, F., Huang, B., & Ding, Z. (2016). A high-resolution geochemical record from the Kuche depression: constraints on early Miocene uplift of south tian Shan. *Palaeogeography, Palaeoclimatology, Palaeoecology*, 446, 1-10. doi.org/10.1016/j.palaeo.2016.01.02
- Thamó-Bozsó, E., Kercsmár, Z., & Nádor, A. (2002). Tectonic control on changes in sediment supply: Quaternary alluvial systems, Körös sub-basin, SE Hungary. *Geological Society, London, Special Publications*, 191(1), 37-53. doi.org/10.1144/GSL.SP.2002.191.01.04
- Thompson, R., & Oldfield, F. (1986). Environmental magnetism, (p. 227). London: Allen and Unwin.
- Wan, S. M., Clift, P. D., Li, A. C., Li, T. G., & Yin, X. B. (2010). Geochemical records in the South China Sea: Implications for East Asian summer monsoon evolution over the last 20 Ma. *Geological Society, London, Special Publications*, 342(1), 245– 263. doi.org/10.1144/SP342.14
- Winters, W. J., Wilcox-Cline, R. W., Long, P., Dewri, S. K., Kumar, P., Stern, L., & Kerr, L. (2014). Comparison of the physical and geotechnical properties of gas-hydrate-bearing sediments from offshore India and other gas-hydrate-reservoir systems. *Marine and petroleum geology*, 58, 139-167. doi.org/10.1016/j.marpetgeo.2014.07.024
- Xiao, R., Zheng, Y., Liu, X., Yang, Q., Liu, G., Xia, L., Bian, Z. J., Feng, G.P., Xu, H., Clift, P.D., Qiang, X., Zhang, Y., & H. Zheng (2021). Synchronous sedimentation in Gonjo Basin, southeast Tibet in response to India-Asia collision constrained by magnetostratigraphy. *Geochemistry, Geophysics, Geosystems*, 22, e2020GC009411. https://doi.org/10.1029/2020GC009411
- Yang, R., Yang, Y., Fang, X., Ruan, X., Galy, A., Ye, C., Meng, Q., & Han, W. (2019). Late Miocene intensified tectonic uplift and climatic aridification on the northeastern Tibetan Plateau: Evidence from clay mineralogical and geochemical records in the Xining Basin. *Geochemistry, Geophysics, Geosystems*, 20(2), pp.829-851. doi.org/10.1029/2018GC007917
- Yang, Y. B., Fang, X. M., Galy, A., Jin, Z. D., Wu, F. L., Yang, R. S., Zhang, W., Zan, J., Liu, X., & Gao, S. (2016). Plateau uplift forcing climate change around 8.6 Ma on the northeastern Tibetan Plateau: Evidence from an integrated sedimentary Sr record. *Palaeogeography, Palaeoclimatology, Palaeoecology*, 461, 418– 431. doi.org/10.1016/j.palaeo.2016.09.002
- Young, G. M., & Nesbitt, H. W. (1998). Processes controlling the distribution of Ti and Al in weathering profiles, siliciclastic sediments and sedimentary rocks. *Journal of Sedimentary research*, 68(3), 448-455. doi.org/10.2110/jsr.68.448

Zhang, M., Lu, H., Guan, H., Liu, L., Wu, D., & Wu, N. (2018b). Methane seepage intensities traced by sulfur isotopes of pyrite and gypsum in sediment from the Shenhu area, South China Sea. *Acta Oceanologica Sinica*, 37(7), 20-27. doi.org/10.1007/s13131-018-1241-1

Zhang, P., Qiu, H., & Mei, L. (2015). Multi-phase Uplift of the Indo-Burman Ranges and Western Thrust Belt of Minbu Sub-basin (West Myanmar): Constraints from Apatite Fission Track Data. *American Geophysical Union, Fall Meeting*, abstract id. T13C-3025.

Zhang, T., Han, W., Fang, X., Miao, Y., Zhang, W., Song, C., Wang, Y., Khatri, D.B. and Zhang, Z. (2018a). Tectonic control of a change in sedimentary environment at~ 10 Ma in the northeastern Tibetan Plateau. *Geophysical Research Letters*, 45(14), pp.6843-6852. doi.org/10.1029/2018GL078460

Zhang, F., Jin, Z., West, A.J., An, Z., & Hilton, R.G., Wang, J., Gen Li, Densmore, A.L., Yu, J., Qiang, X., Sun, Y.B., Li, L.B., Gou, L.F., Yang, Xu., Xinwen, Xu., Liu, X., Pan, Y., & You, C.F. (2019). Monsoonal control on a delayed response of sedimentation to the 2008 Wenchuan earthquake. *Science Advances*. 5: eaav7110. Doi: 10.1126/sciadv.aav7110.

Table-01: Depth-wise distribution of iron sulfide nodules in sediment core NGHP-01-17A

Sr. No.	Nodule No.	Core depth Interval (mbsf)
1.	AN-01	31.56
2.	AN-02	31.98
3.	AN-03	32.22
4.	AN-04	35.07
5.	AN-05	36.83
6.	AN-06	40.50
7.	AN-07	40.49
8.	AN-08	40.61
9.	AN-09	40.63
10.	AN-10	40.65
11.	AN-11	41.08
12.	AN-12	41.13
13.	AN-13	41.94
14.	AN-14	42.03
15.	AN-15	43.59
16.	AN-16	43.61
17.	AN-17	44.57
18.	AN-18	48.46

Figure -1: (a) Bathymetric map of Andaman Sea and the sediment core location (NGHP-01-17A) (modified after Awasthi et al., 2014), (b) Down-core variation in sediment magnetic susceptibility record of NGHP-01-17A, and (c) General geological map of the Andaman Sea sediment source regions modified after Guo et al. (2016). Sediment magnetic zones are marked by red (Z-I) and blue (Z-II) color line respectively. The depth of sulfate-methane transition zone (SMTZ) is marked by the dotted (pink color) line.

Figure-2: Multi-proxy sediment record of core NGHP-01-17A (a-d) rock magnetic (χ_{lf} , SIRM, ARM/SIRM, S-ratio), (e) Sedimentology (mean grain size), (f-h) Geochemical (TOC, Fe and CaCO_3 content) parameters, (i) Physical property (sediment electrical resistivity; data taken from NGHP Expedition-01 report; Collet et al., 2008), and (j) Ice volume corrected $\delta^{18}\text{O}_{sw}$ record (Gebregiorgis et al., 2018). Sediment magnetic zones are marked by red (Z-I) and blue (Z-II) color line respectively. Please note that four low S-ratio zones are marked as S1, S2, S3, and S4. Distribution of volcanic ash layers (sampled from sediment core) are indicated by arrows (light blue color). Timings of tectonic events and uplift of the NE Tibetan Plateau are presented and marked by dashed lines (for details please see Li and Fang, 1999; Li et al., 2014; Qingsong Z, 2000). Episodes of Kunlun–Huanghe (Yellow River) Movement (KHM, 150 Ka) and Gonghe Movement (GHM, 1200 ka – 600 ka) are mentioned.

Figure-3: Temperature-dependence of magnetic susceptibility (χ -T) for selected representative sediment samples (a-d): Zone-I and (e-h) Zone-II of core NGHP-01-17A. Solid red lines indicate heating curves, and blue lines indicate cooling curves.

Figure-4: Vertical distribution of (a) magnetic susceptibility (χ_{lf}), (b) calcium carbonate content, (c-f) selected major element compositions of sediments and (g-h) elemental ratios in the core NGHP-01-17A.

Figure-5: Scanning electron microscope images (secondary electron) on magnetic extracts representative of two different sediment magnetic zones (a-b: Zone-I and c-g: Zone-II) of core NGHP-01-17A. Energy dispersive X-ray spectroscopy spectra are placed adjacent to the respective images (a–g). Iron (Fe), titanium (Ti), sulfur (S), oxygen (O), calcium (Ca), silicon (Si), carbon (C), aluminum (Al) and magnesium (Mg) peaks are indicated.

Figure-6: X-ray diffraction spectra for selected representative bulk sediment samples of core NGHP-01-17A: Zone-I (a,b,g,h) and Zone-II (c,d,e,f,i,j,k,l) of core NGHP-01-17A. M = magnetite, Py = pyrite, Qz = quartz, Calcite = Ct, H=Hematite.

Figure-7: (a-f) X-ray diffraction spectra for selected iron sulfide nodules picked from core NGHP-01-17A. Qz = quartz, S=Sulfur, G = Gypsum, Py = pyrite, Al=aluminium.

Figure-8: (a) magnetic susceptibility (χ_{lf}) (b) pore-water sulfate (c) methane gas profile of sediment core NGHP-01-17A. (d-f) microscopic images of iron sulfide nodules, (g-i) scanning electron microscope images (secondary electron) of iron sulfide nodules. (j–l) energy dispersive x-ray spectra are placed close to the respective images. Iron (Fe), sulfur (S), oxygen (O), silicon (Si), carbon (C), aluminum (Al) peaks are indicated. Brown color dashed lines indicates the depth of nodule occurrence. Pore-water sulfate and methane gas data of core NGHP-01-17A was taken from NGHP Expedition-01 report (Collet et al., 2008).

Figure-9: (a-c): Bivariate scatter plots of magnetic parameters: magnetic susceptibility (χ_{lf}), saturation isothermal remanent magnetization (SIRM), anhysteretic remanent magnetization ARM/SIRM, and S-ratio), (d) χ_{lf} versus mean grain size, (e) ARM/SIRM versus mean grain size, (f) χ_{lf} versus iron content (Fe %) content, (g) Fe/K versus χ_{lf} , and (h) Ti/Al versus χ_{lf} . Samples from group-A are distinctly marked by relatively higher χ_{lf} , Fe, Fe/K, Ti/Al and relatively lower ARM/SIRM values compared to group-B samples. Clusters of group-A and group-B samples are highlighted in light blue and light green color respectively in Figure 9g and 9h. Note that gray arrows in the scatter plots are used only to highlight trends.

Figure-10: (a-b): A plausible mechanism explaining the controls on the evolution of sedimentary magnetic zones (Z-I, Z-II) in the Andaman Sea over the past ~ 1 Ma.

Supplementary Figures:

Figure S1. Age-depth model for sediment core NGHP-01-17A. Age model was developed based on AMS ^{14}C dates on planktonic foraminifera by Gebregiorgis et al. (2018). Age depth model indicating a near linear sedimentation rate.

Figure S2. A bivariate plot between χ_{lf} and χ_{ARM} exhibiting the grain-size control on the iron bearing sediments (King's plot).

Figure. 1

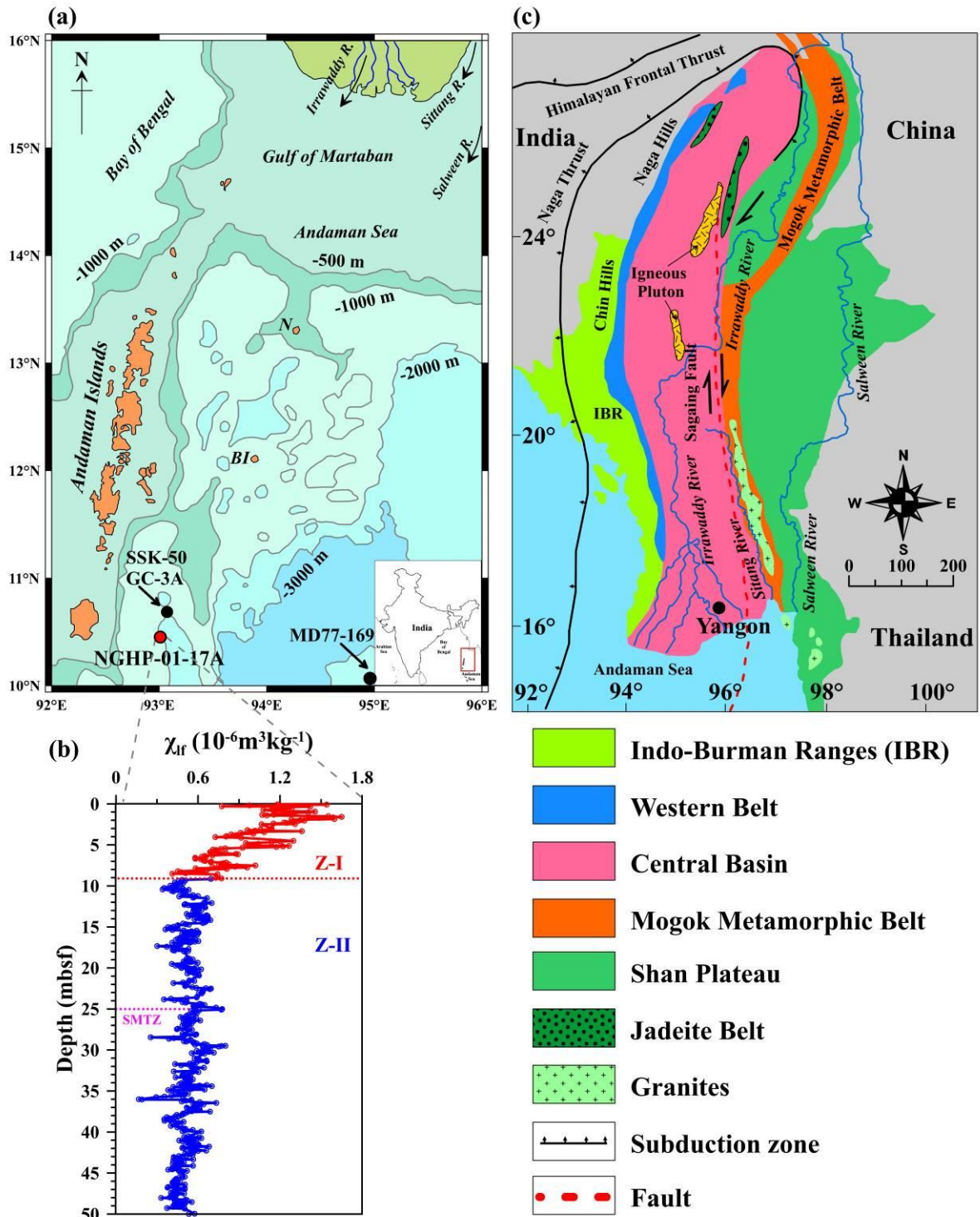


Figure. 2

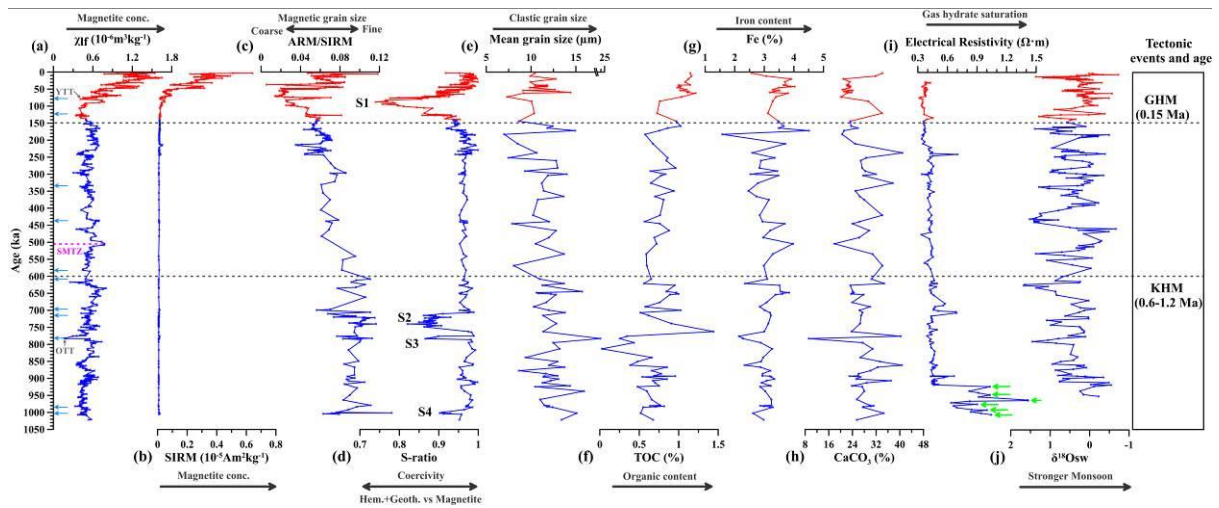


Figure. 3

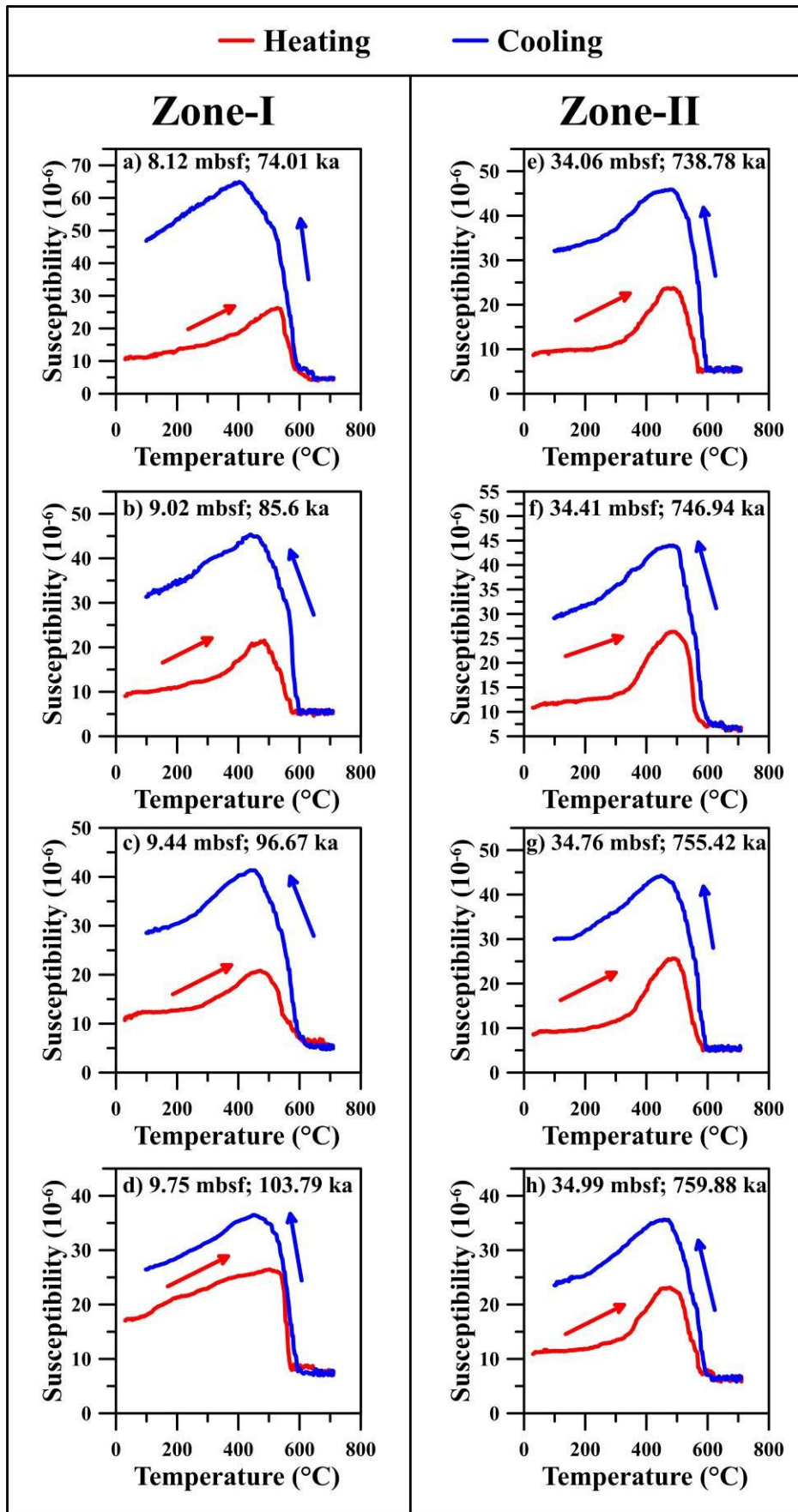


Figure. 4

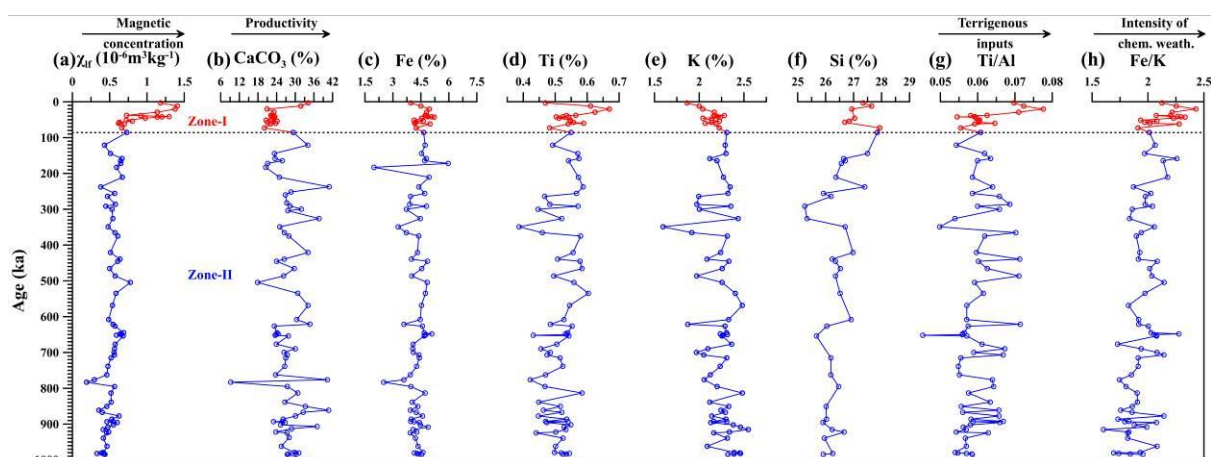


Figure. 5

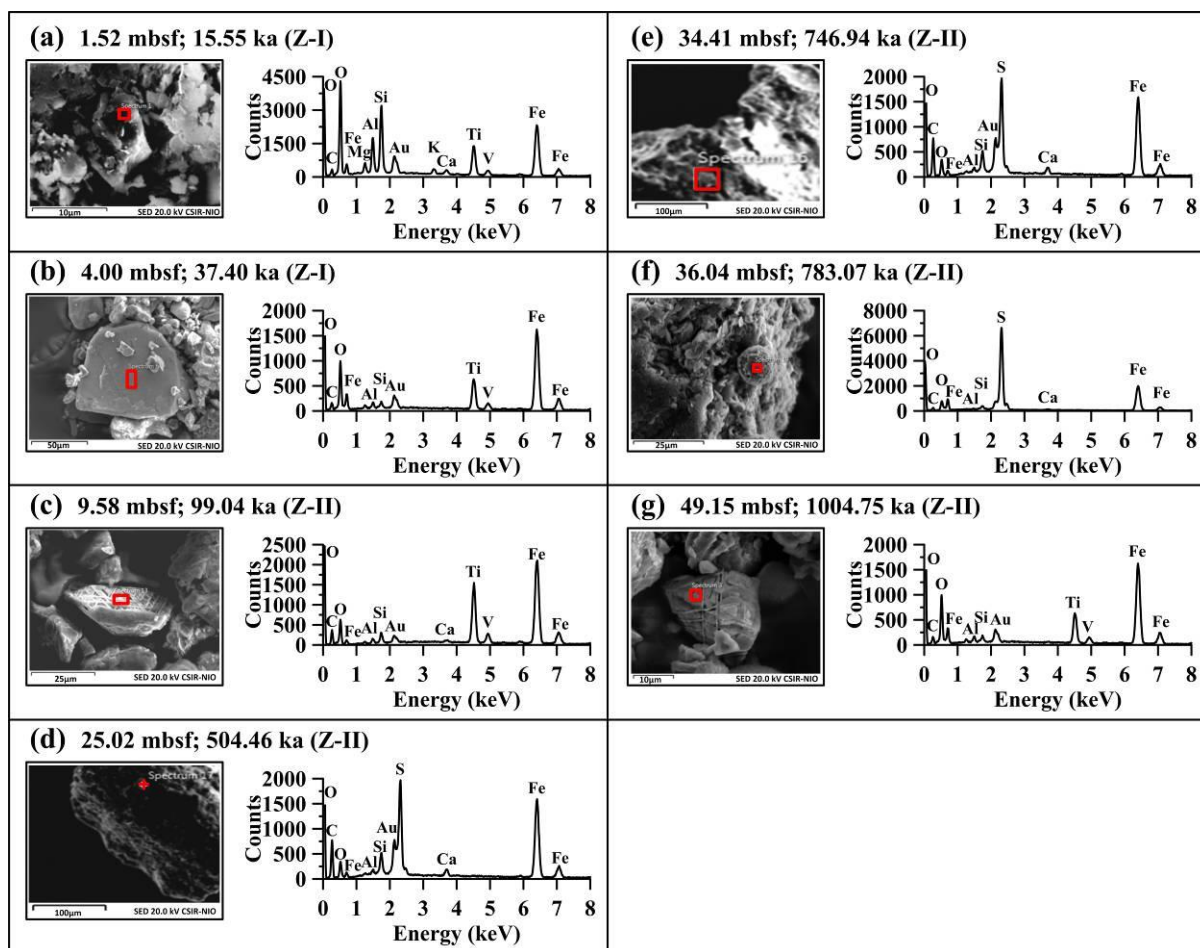


Figure. 6

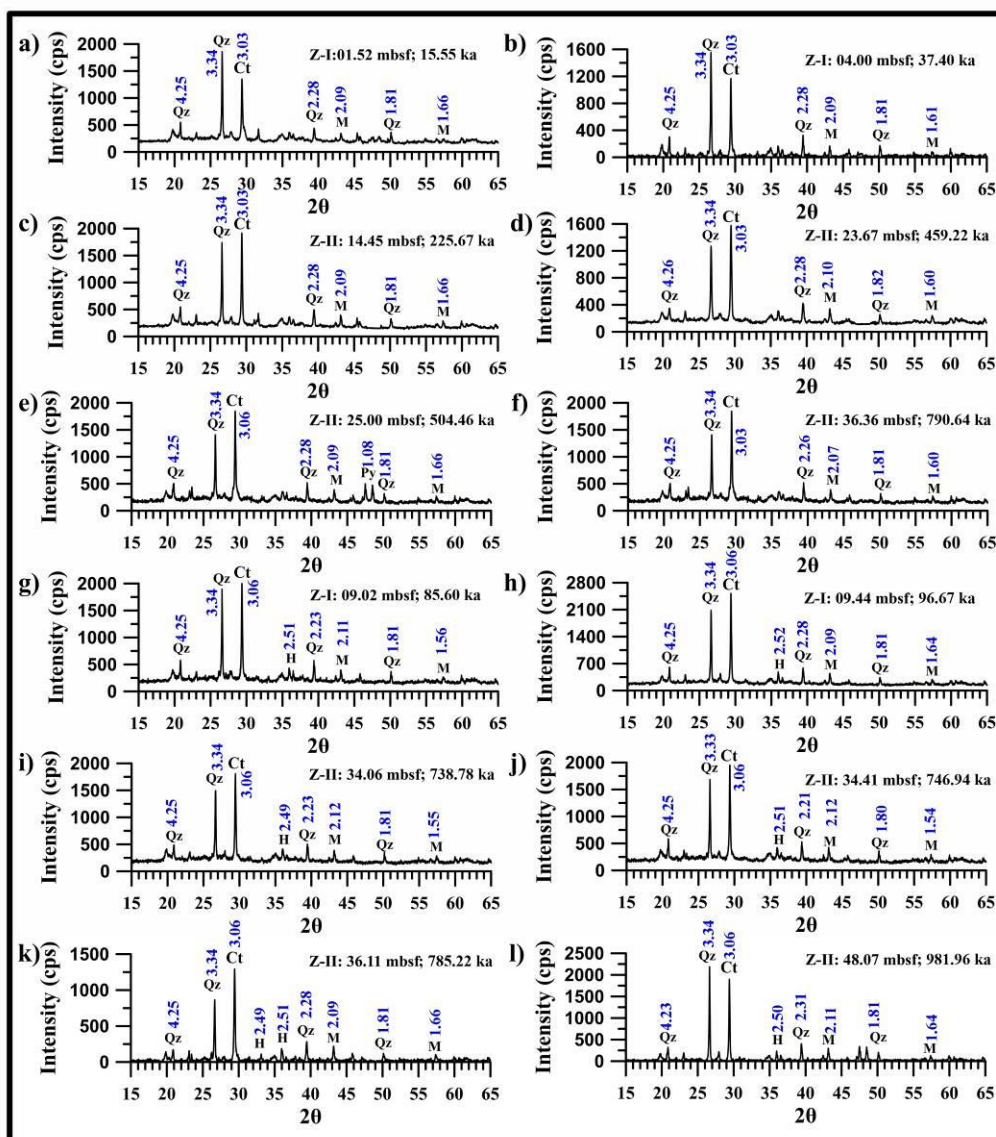


Figure.7

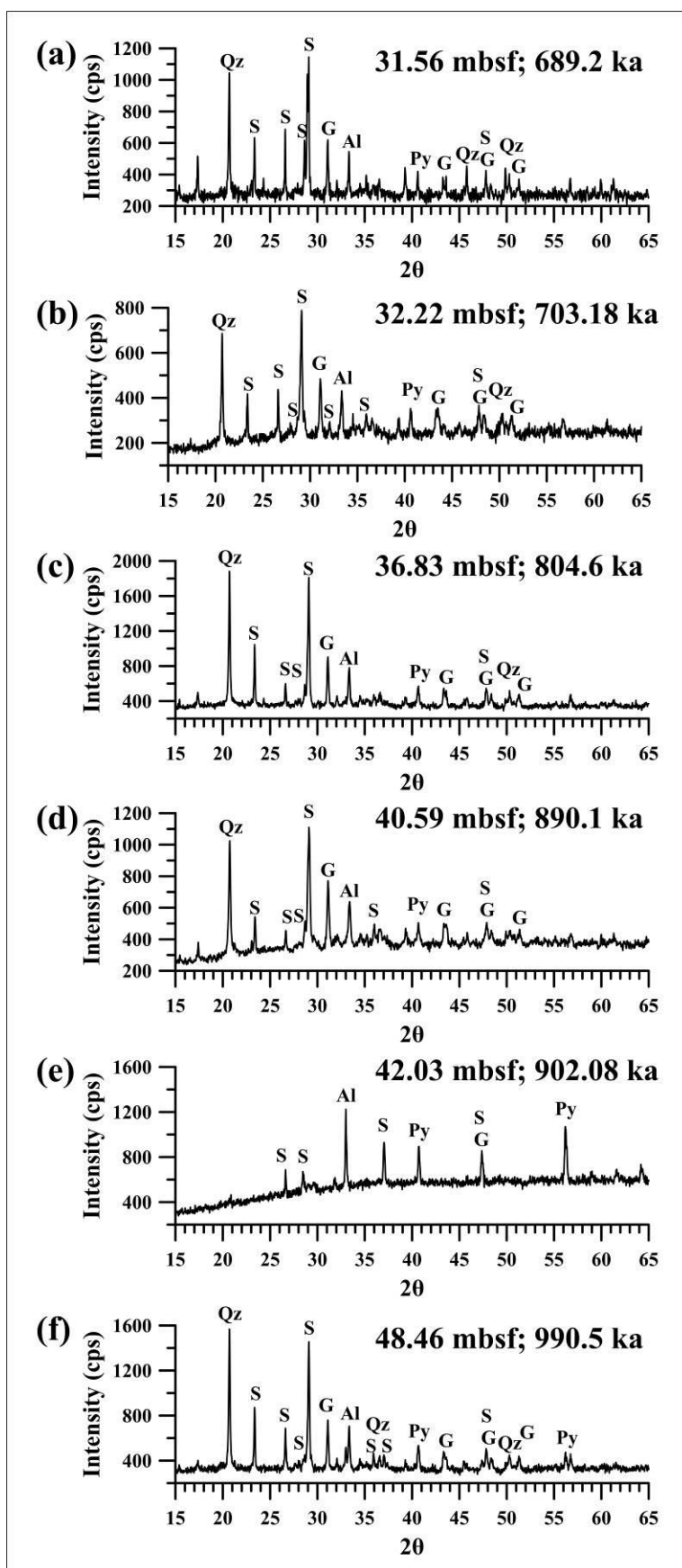


Figure. 8

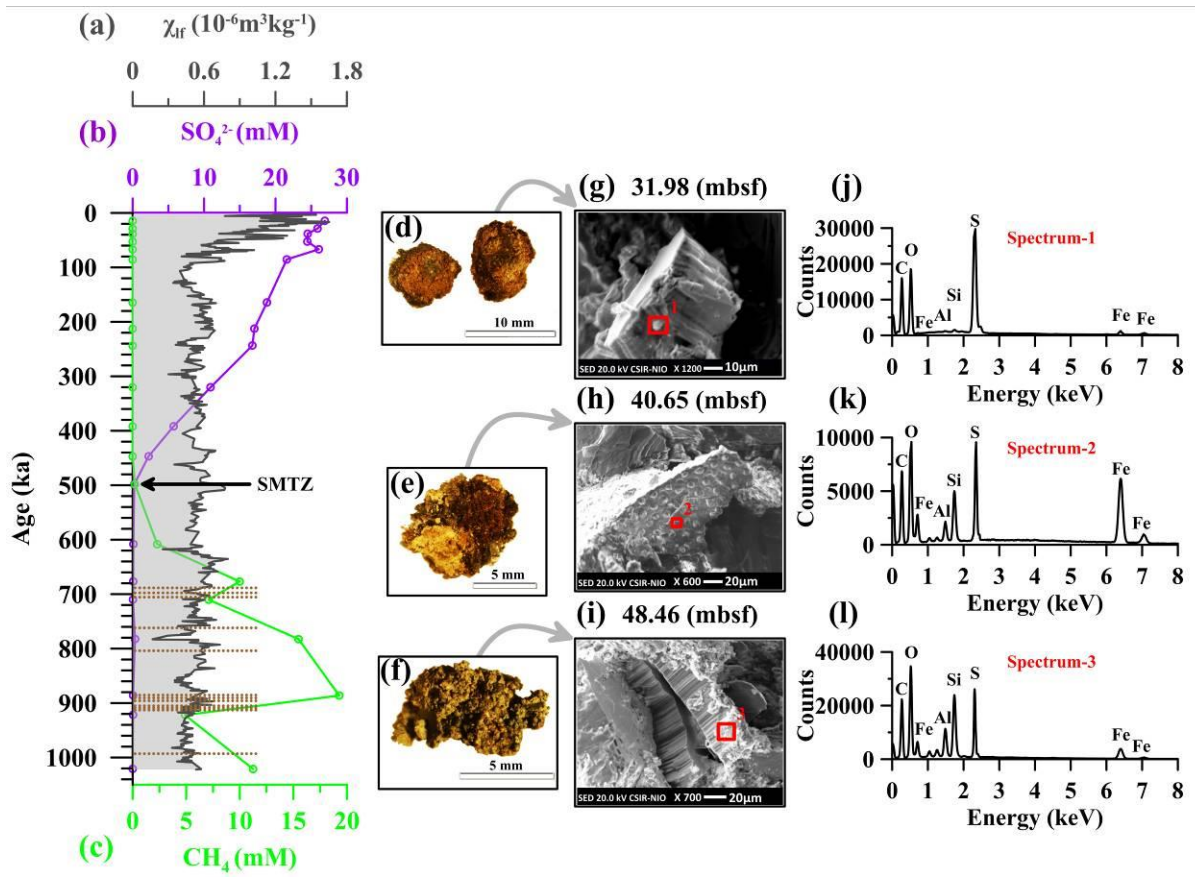


Figure. 9

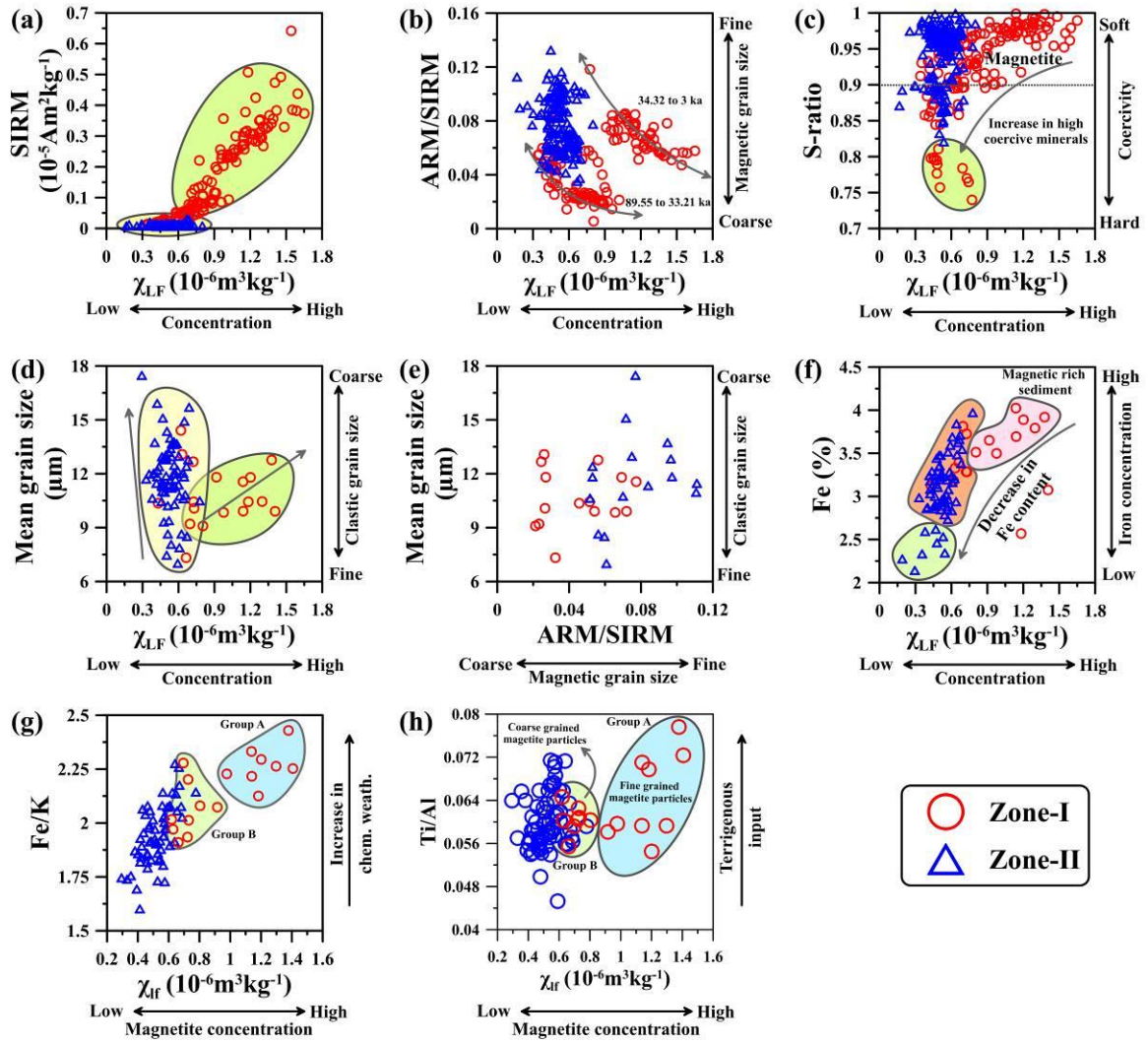


Figure. 10

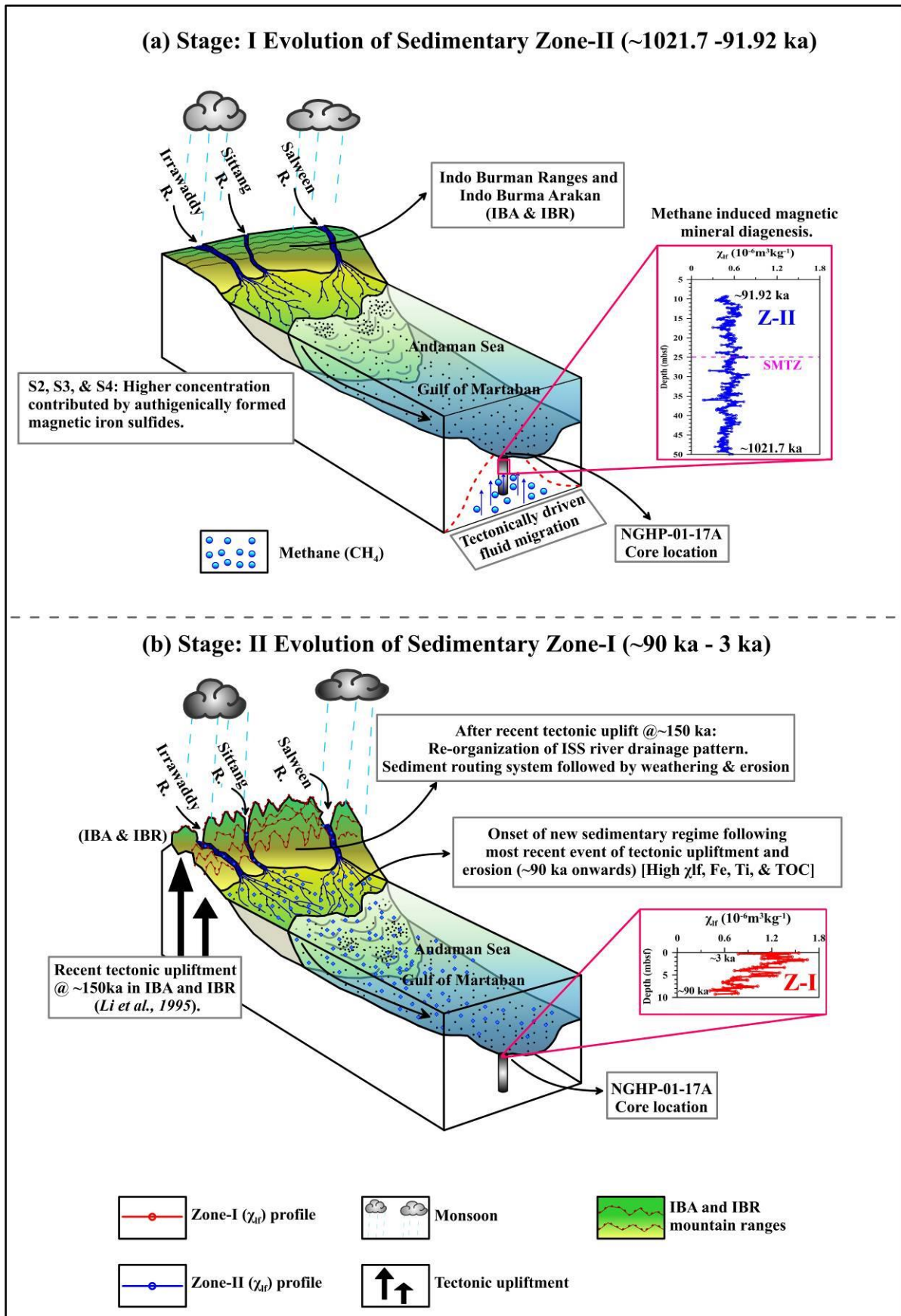


Figure. S1

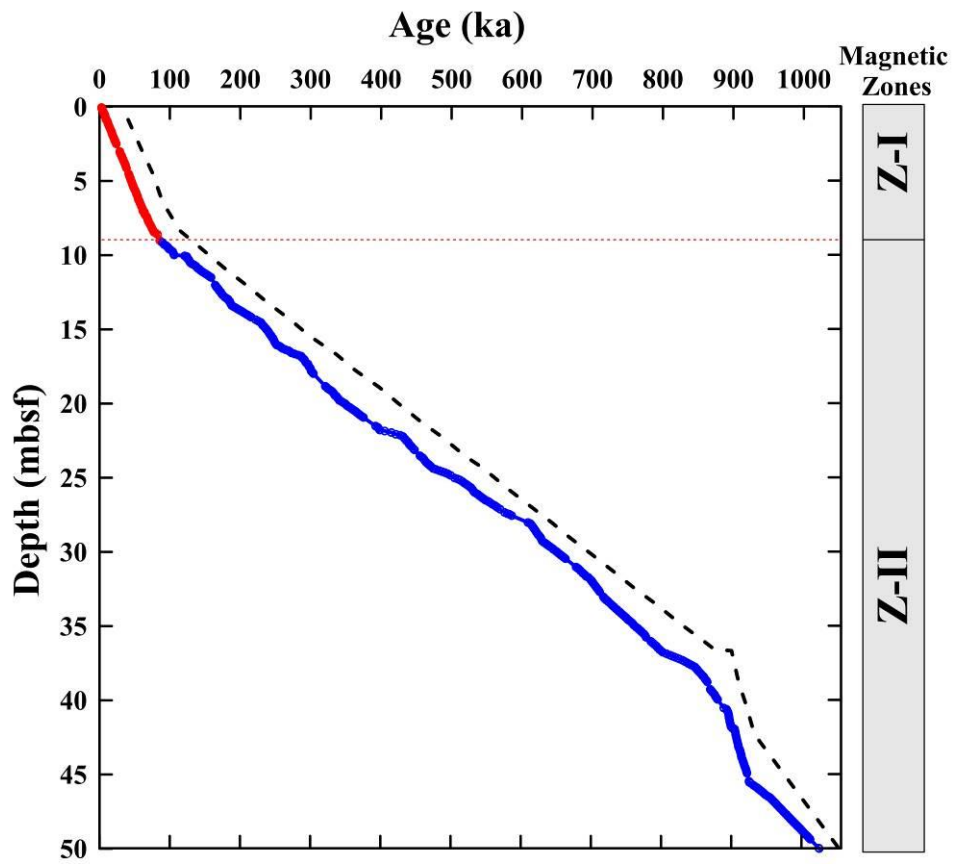


Figure. S2

